P-041

Y

Real-time monitoring of the cytidine deamination along single-stranded DNA by an anti-HIV factor, APOBEC3G

Ayako Furukawa[1], Kenji Sugase[2], Ryo Morishita[3],Takashi Nagata[1], Akihide Ryo[4], Akifumi Takaori[5] and Masato Katahira[1]
[1]Inst. of Adv. Energy, Kyoto Univ., [2]Bioorg. Res. Inst., Suntory Found. Life Sci., [3]CellFree Sci., [4]Grad. Sch. Med., Yokohama City Univ., and [5]Grad. Sch. Med., Kyoto. Univ.

Introduction

Human APOBEC3G (A3G), an anti-HIV-1 host factor, deaminates cytidine in the minus-strand of the HIV DNA so that the HIV replication can ultimately be inhibited. A3G preferentially deaminates the third cytidine of a CCC hotspot sequence in a single-strand DNA (ssDNA). Although A3G is a potential target for HIV therapy, the mechanism of the deamination reaction is still poorly understood. In this study, we monitored the cytidine deamination reaction using real-time NMR,[1] and fitted the data to newly constructed kinetic models in order to obtain insight into the mechanism of A3G deamination reaction.

Results and Discussions

A3G has two cytidine deaminase domains, but only the C-terminal domain (A3G-C: residues 193-384) is involved in the catalytic activity. Previous biochemical studies showed that full-length A3G has 3'→5' deamination polarity but A3G-C has no polarity preference. Firstly, we have quantitatively analyzed the deamination activity and polarity of A3G and A3G-C using real-time NMR that we developed[1]. Multiple TOCSY spectra were continuously acquired to monitor the conversion from cytidine to uridine on a ssDNA containing two CCC hotspots. After the addition of A3G, uridine peak appears as cytidine peak disappears (Fig. 1). We chased the intensity changes of the cytidine peaks in real time. To our surprise, real-time NMR revealed that A3G-C deaminates cytidine with a strong 3'→5' polarity and the reaction rate of A3G-C is comparable to that of A3G. Therefore, we concluded that A3G-C is the determinant for the deamination polarity and rate, and

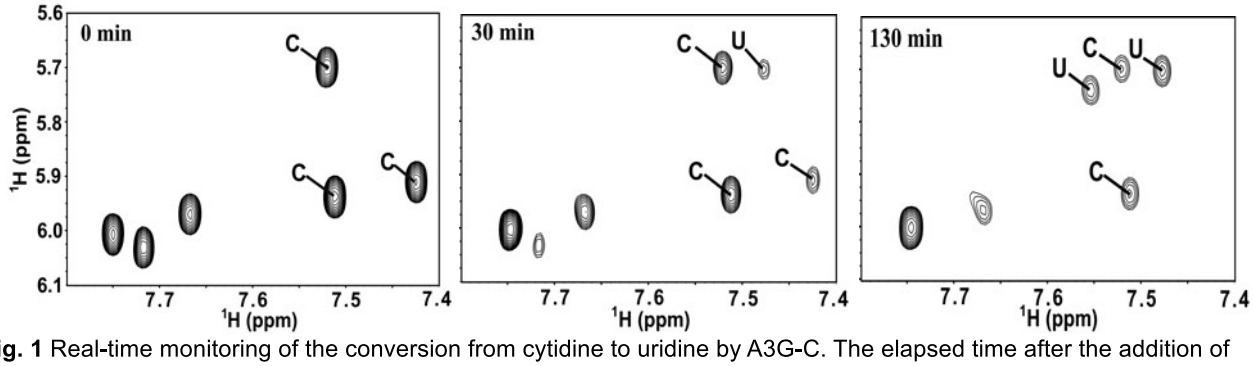

Fig. 1 Real-time monitoring of the conversion from cytidine to uridine by A3G-C. The elapsed time after the addition of A3G-C is indicated at the top left corner of each spectrum.

thus we used only A3G-C in all the subsequent experiments.

In order to further obtain the details of the 3'→5' polarity of the deamination reaction by A3G-C, we measured the deamination rates of three CCC hotspots, each of which was contained separately in a ssDNA with the same length but the position was different: near 5' end, in the center and near 3'

end. As shown by Fig. 2, the order of the deamination rates was near 5' end > in the center > near 3' end. Namely, CCC hotspots in the upstream regions, or 5'-side regions, have higher deamination rates. Here, we hypothesized that the cytidine deamination by A3G-C is coupled to 3' → 5' sliding. The hypothesis was confirmed by an experiment using a ssDNA containing a short double-strand region in the middle of two CCC hotspots. In the experiment, the deamination rates for the two hotspots were almost the same whereas the rate was faster for the 5' side when just the ssDNA was used. The results indicate that A3G certainly slides on a ssDNA, and the sliding is precluded by the double-stranded region.

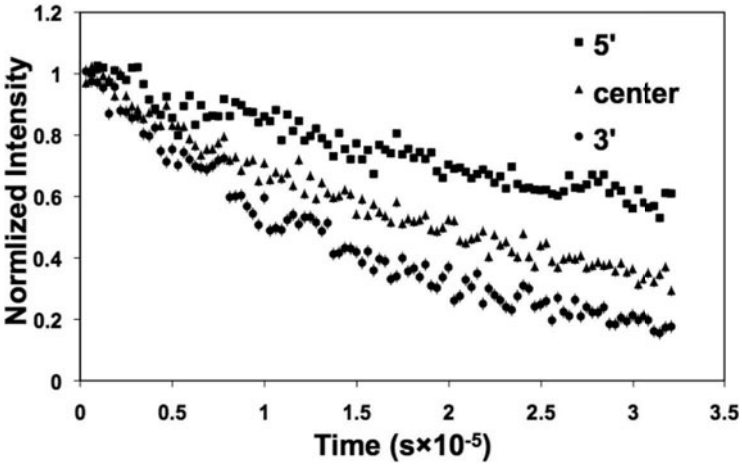

Fig. 2 Location dependence of the deamination reaction by A3G-C

Next, we asked how A3G-C exerts the 3' →5' deamination polarity. Here, we propose two kinetic models for the coupled deamination and sliding on a ssDNA. In Model 1, the sliding rates from 3' to 5', $k_{s(3' \rightarrow 5')}$, and from 5' to 3', $k_{s(5' \rightarrow 3')}$ are defined to be different, but the associated catalytic reaction rates were same. In Model 2, A3G sliding has no directional preference, but the deamination is direction dependent with different catalytic reaction rates, $k_{cat(3' \rightarrow 5')}$ and $k_{cat(5' \rightarrow 3')}$. In both models, we assume that A3G-C sliding is caused by Brownian motion, and A3G-C does not change its direction when sliding on a ssDNA. We derived theoretical equations for these models. and fitted the real-time NMR data to the theoretical equations. As a result, we obtained intrinsic dissociation constant, K_d (= k_{off}/k_{on}), catalytic reaction rate(s), and ratio(s) of the sliding rate(s) to the dissociation rate, k_{off}. Model 2, where the direction from which A3G-C enters into the hotspot, fitted the data very well and the polarity, $k_{cat(3' \rightarrow 5')}$ was determined to be 4 times faster than $k_{cat(5' \rightarrow 3')}$. This model seems physiologically reasonable because the sliding probabilities for both directions should be equal in Brownian motion, and the difference in the catalytic rates is expected to be caused by the asymmetric structure of A3G-C. Analysis of Model 1is currently in progress.

In this study, we have demonstrated that real-time NMR is a powerful tool to elucidate the mechanism of the cytidine deamination by A3G, which is coupled to 3' →5' sliding. Further analysis would shed light on a future HIV therapy targeting A3G.

References

1) Furukawa, A., *et al* (2009) *EMBO J.* **28**, 440-451.

---

real-time NMR, sliding on ssDNA, deamination reaction

P-042

Y

Structural analysis of a non-coding RNA, CeR-5, found in *C. elegans*

Tomonori Yoshida[1], Tatsuya Shimane[1], Takafumi Kawaguchi[1], Seiki Fujiwara[2], Yuki Sugawara[2], Chisato Ushida[2] and Gota Kawai[1]
[1]Department of Life and Environmental Sciences, Chiba Institute of technology, [2]Department of Biochemistry and Molecular Biology, Hirosaki University

ABSTRACT

CeR-5 is a novel non-coding RNA found in *C. elegans*. It was found that CeR-5 is expressed in almost all cell thoughout the life cycle of *C. elegans*. However, the secondary and tertiary structure as well as the function of CeR-5 is not known yet. Because CeR-5 is a rather long RNA (132 nt) for NMR analysis, we designed a 40-mer RNA (CeR-5m) corresponding to region where a stable secondary structure was predicted. We compared the NMR spectra of CeR-5 and CeR-5m and found that CeR-5m and CeR-5 share the stem structure which was predicted CeR-5.

INTRODUCTION

Recently, it was revealed that large number of non-coding RNAs (ncRNAs) are expressed in cells and play various and important biological roles. Most of ncRNAs are expected to form stable tertiary structures for their function and, thus, structure determination of each ncRNA is quite important to elucidate the function of the ncRNA.

Eight novel non-coding RNAs (ncRNAs) that were encoded in the regions corresponding to the introns of protein-coding genes were isolated from *C. elegans*. Seven of them showed a typical snoRNA secondary structure: one C/D snoRNA and six H/ACA snoRNAs. The remaining RNA (CeR-5; Fig. 1a) did not show any homology to other RNAs. It was found that CeR-5 is expressed in almost all cells throughout the life cycle of *C. elegans*. As for the intracellular localization, it has been revealed that the majority of CeR-5 exists in the nucleolus and an significant amount of the RNA also exists in the nucleoplasm. In order to elucidate the function of CeR-5, it is important to know the tertiary structure of CeR-5. Thus, we started NMR analysis of CeR-5.

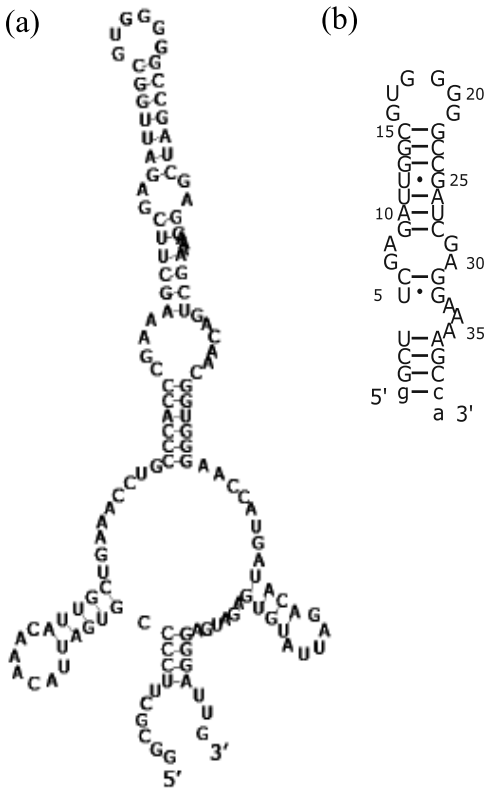

Fig. 1 Secondary structure of CeR-5 (a) and CeR-5m (b)

RNA

RESULTS AND DISCUSSION

Design of a substructure CeR-5m

Since CeR-5 is a rather long RNA (132 nt) for NMR analysis, we designed a 40 mer RNAs (CeR-5m, Fig. 1b) corresponding to the long stem-loop region of CeR-5 as the first target of the structure determination. The results of RNA secondary structure predictions with vsfold4 and mfold suggested that CeR-5m forms the same secondary structure with CeR-5 as shown in Fig. 1. In order to confirm the formation of the secondary structures, we prepared the CeR-5 and CeR-5m RNAs by *in vitro* transcription with T7 RNA polymerase and compared the imino proton spectra of those RNA samples to each other (Fig. 2). Although the signals for CeR-5 are not assigned yet, most of imino proton signals observed for CeR-5m were found in the spectrum of CeR-5 indicating that these RNA share similar secondary and tertiary structures.

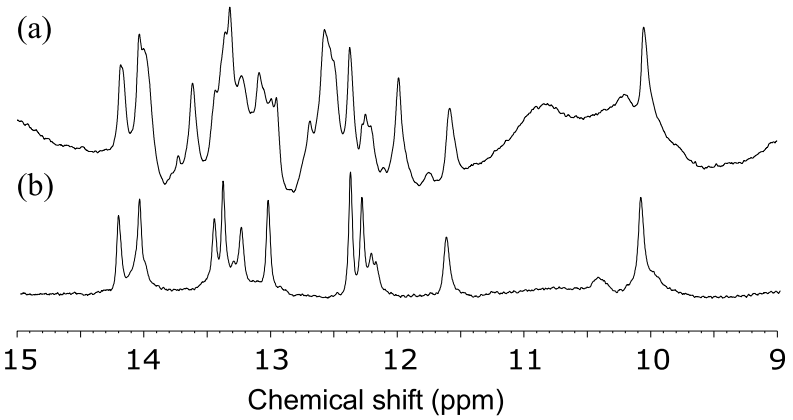

Fig. 2 Imino proton spectra of CeR-5 (a) and CeR-5m (b) observed in 5% D2O at 298 K

NMR analysis of CeR-5m

Fig. 3 shows the NOESY spectrum of CeR-5m observed in 5% D_2O at 283 K. The sample concentration was 0.48 mM and DRX-600 spectrometer (Bruker) was used. The strong NOE between signals at 10.0 and 11.6 ppm was typical for U-G base pairs and the two signals were assigned to U13 and G25, respectively. Based on the NOE connectivity including the signals due to the U-G pair, most of imino proton signals were tentatively assigned, confirming that CeR-5m takes the predicted secondary structure as shown in Fig. 1b. This result is also indicating that the CeR-5 takes the predicted secondary structure at least in the long stem-loop region.

In order to elucidate the structure of CeR-5m, further NMR analysis including stable isotopic labelling is in progress.

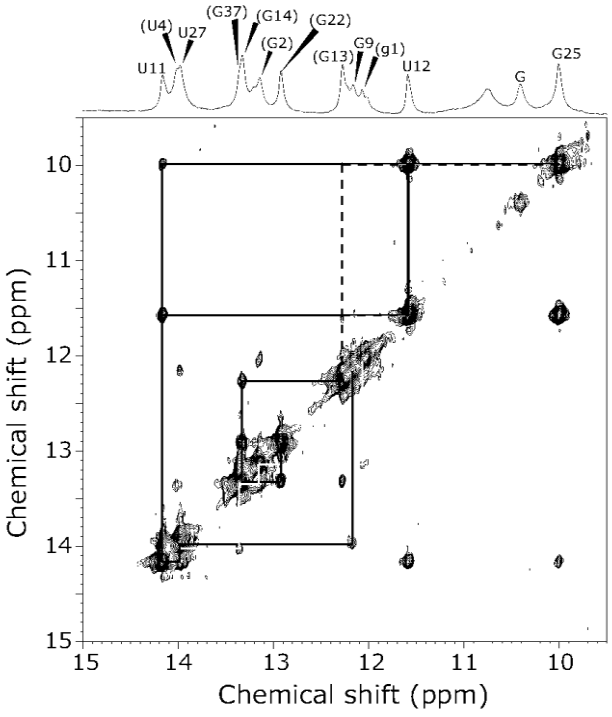

Fig. 3 NOESY spectrum of CeR-5m Tentative assignments were shown on the top

REFERENCES

1) Wachi, M. Ogawa, T., Yokoyama, K., Hokii, Y., Shimoyama, M., Muto, A. and Ushida, C. (2004) *Gene* **335**, 47-56.

P-043 Structural analyses of receptor recognition mechanism of a mouse pheromone ESP1

Makoto Hirakane[1], Sosuke Yoshinaga[1], Toru Sato[2], Sachiko Haga[2], Ichio Shimada[3], Kazushige Touhara[2], Hiroaki Terasawa[1]

[1]Faculty of Life Sciences, Kumamoto University, [2]Graduate School of Agricultural and Life Sciences, The University of Tokyo and [3]Graduate School of Pharmaceutical Sciences, The University of Tokyo

Pheromones are essential for social communication in many species. In mice a male-specific peptide ESP1 is secreted into tear fluids and received by V2Rp5, which is a GPCR expressed in female VSNs. The aim of this study is to elucidate the molecular mechanism underlying the pheromone reception system and the clarification of the structural basis of the GPCR activation. We determined an NMR solution structure of ESP1 and performed protein interaction analyses between ESP1 and V2Rp5. We also proposed a complex model of ESP1 and V2Rp5, using a docking simulation based on biological assays *in vivo* and *in vitro*. The structure-activity relationship of ESP1 based on the structural data and biological analyses will be discussed.

Introduction

Pheromones are species-specific chemical signals that regulate a wide range of social and sexual behaviours in many animals. Mice detect pheromones through vomeronasal sensory neurons (VSNs) in the vomeronasal organ (VNO), a secondary olfactory system that detects pheromonal information, regarding a range of factors such as sex, strain, and species. We have identified a male-specific peptide ESP1 (exocrine-gland-secreting peptide 1) secreted into tear fluids that stimulates female VSNs[1)]. ESP1 is now known to be a member of a multigene family. The ESP family consists of 38 and 10 genes in mice and rats, respectively[2)]. In addition, The ESP1 signal is received by the vomeronasal type 2 receptor p5 (V2Rp5). V2Rp5 is a class C G protein-coupled receptor (GPCR) expressed in VSNs[3, 4)] and has the long N terminal domain. Recently, we revealed that ESP1 enhances female sexual receptive behaviour upon male mounting (lordosis), allowing successful copulation[4)]. ESP1 is the first mammalian peptidic pheromone for which a ligand, a receptor and a function has been discovered. The purpose of this study is the elucidation of the mechanism to discriminate among individuals via the pheromone reception system and the clarification of the structural basis of the GPCR activation based on NMR and biological analyses.

Materials and Methods

All NMR data were processed using the NMRPipe software system and were analyzed using the Olivia software. Structural calculations of ESP1 were performed using the CYANA

ESP1, GPCR, molecular recognition

programme. We examined the induction of c-Fos as a marker for activated VSNs after stimulation with ESP1 according to the procedure reported by Kimoto *et al.* [1]. Using the wheat germ cell-free protein synthesis system, the extracellular region of V2Rp5 was produced. To perform *in vitro* pull-down assays, ESP1 was covalently coupled to derivatized agarose-gel beads. V2Rp5 was incubated with ESP1-coupled beads and bound V2Rp5 was eluted with buffer containing free ESP1 or ESP4. In a separate experiment, Bound V2Rp5 was eluted with the same buffer containing 500 mM NaCl. A V2Rp5 model was constructed with MOE software. A complex model was built based on the electrostatic surface potentials of ESP1 and V2Rp5 model.

Results and Discussion

We determined the solution NMR structure of ESP1. ESP1 consists of three helices and has a large positively charged patch on its surface. Charged amino acids of the molecular surface of ESP1 were mutated. We examined the effects of the mutations on the VSNs-stimulating activity of ESP1, using c-Fos expression. Several mutants lost c-Fos activity. The data suggested that charged amino acids on the surface of ESP1 are important for the activity. We performed *in vitro* pull-down assays to determine whether ESP1 directly interacts with the extracellular region of V2Rp5. V2Rp5 which bound to ESP1-coupled beads was eluted with buffer containing free ESP1 or ESP4. Western blot analysis of the pull-down fractions showed interaction between V2Rp5 and ESP1, but not ESP4. This result demonstrated specific binding of ESP1 to the extracellular region of V2Rp5. V2Rp5 was incubated with ESP1-coupled beads, and eluted with a high salt buffer. V2Rp5 was eluted from ESP1-coupled beads. We clarified that electrostatic interactions are essential for the binding of ESP1 and V2Rp5. We constructed a homology model of V2Rp5, using the structure of the metabotropic glutamate receptor 1 (mGluR1) belonging to class C GPCR as the template, and a structural model of the ESP1-V2Rp5 complex (Fig. 1). The size of ESP1 matches that of the binding site of V2Rp5.

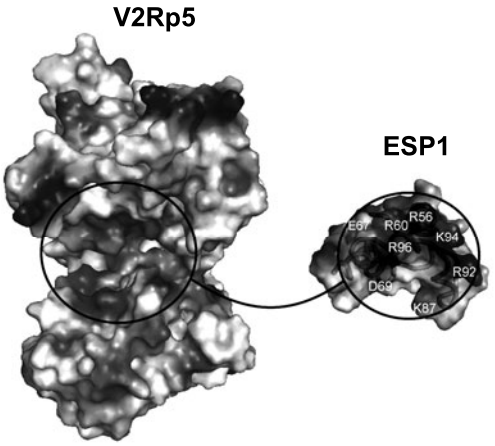

Figure 1 A putative binding surface of the ESP1–V2Rp5 complex, shown as an open-book representation.

We discuss the structure-activity relationship of ESP1 based on the structural data and the effects of mutation on its VSN-stimulating activity, and the ligand-receptor recognition mechanisms of GPCR based on electrostatic interactions.

References

1) Kimoto H. *et al.*, *Nature*, **437**, 898-901 (2005)
2) Kimoto H. *et al.*, *Current Biology*, **17**, 1879-1884 (2007)
3) Haga S. *et al.*, *Pure and Applied Chemistry*, **79**, 775-783 (2007)
4) Haga S. *et al.*, *Nature*, **466**, 118-122 (2010)

P-044 Structural analysis of functional RNA longer than 100 nt by using NMR

Takako Ohyama[1] and Gota Kawai[1]
[1] Department of Life and Environmental Sciences, Chiba Institute of Technology

ABSTRACT
Structural studies of RNA by using NMR are often harder than the cases of protein, because the properties of chemical structure of RNA make difficult to assign their NMR signals. Therefore, longer RNA that has unique structure was broken down to structure units consist of ~ 50 nt to determine their structures in most of previous works. In this work, we will present our strategy and efforts to determine the structures of RNAs that consist of more than 100 nt.

INTRODUCTION
In recent years, a new class of transcripts, long non-coding RNAs (lncRNAs), has been found to be pervasively transcribed in the genome. These RNAs are often contains unique structural domains consisting of 50-300 resides. To elucidate the structures and functions of these newly found lncRNAs on atomic resolution by intact form, it is fundamental to develop a new method for structural analysis of long RNA. Thus, we aim to develop a new method for determination of the structure and dynamics of longer functional RNAs. Our strategy is that (i) extraction of the structural domains from long RNA based on secondary structural analysis, (ii) refinement of the structural region of interest and (iii) structure determination of the RNA fragment corresponding to the structural region of interest. In most case, the RNA fragment is longer than 100 nt and, thus, development of NMR technique to analyze such RNA is quite important.

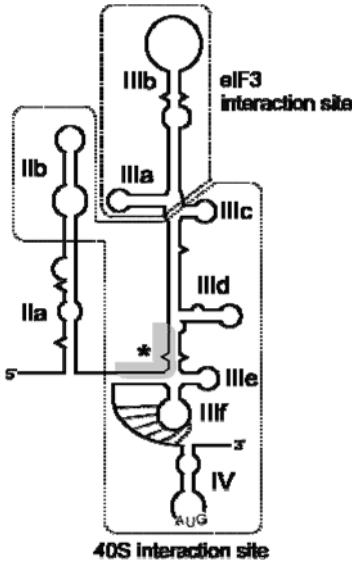

Fig. 1 Secondary structure of the HCV IRES

RESULTS AND DISCUSSION
Extraction of the structural domains from long RNAs
To grasp the secondary structure of long RNA, we are using the program GenoPoemics (GP)[1)]. For the first example of GP analysis, we selected HCV IRES (Fig. 1). HCV IRES is one of well known functional RNA that mediates cap-independent transcription initiation in higher eukaryotes. Fig 2 shows the GP spectrum of HCV genomic RNA and the region of HCV IRES was clearly displayed as the secondary structure rich region including the two major domains, II and III, and both of them are essential for translation initiation activity. Most of tertiary structures of small unit of IRES are detected, but IIIef which is crucial for IRES activity has not been determined.

RNA,

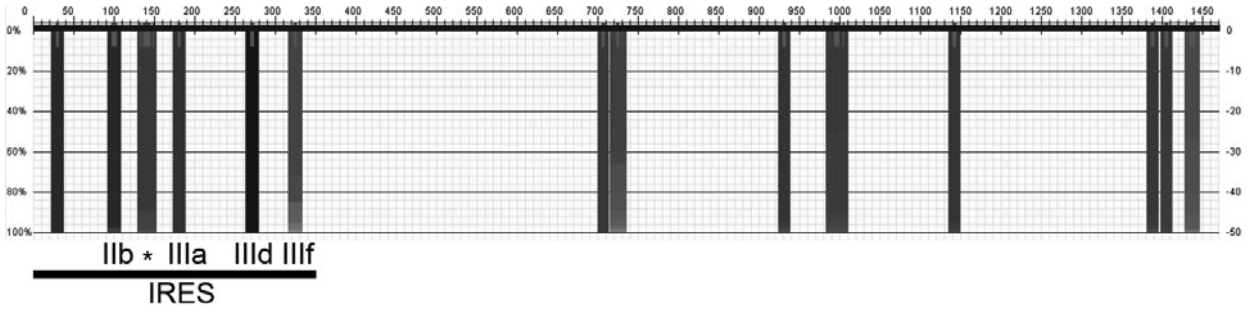

Fig. 2 A GP spectrum of the 5′-region of the HCV genomic RNA

Refinement of the extracted secondary structure

Before starting the structural analysis by NMR, the secondary structure predicted by the GP spectrum must be refined by the precise prediction including pseudoknot with vsfold5[2]. Fig. 3 shows the result of precise secondary structure prediction of HCV IRES by vsfold5. In this case, the pseudoknot (PK), which was not found in the GP spectrum, is predicted as indicated in the figure.

Structure determination of the RNA having more than 100 residues

Conformational analysis of RNA by using NMR contains several difficulties as compared with proteins and DNAs. There are mainly two reasons, one is that RNA has less proton density as compared to protein, and the other is NMR signals of RNA are congested by its nature. Therefore, in practice, the conformational analysis of longer RNA is hard, thus longer RNAs are broken down to structure units and analyzed.

IRES IIIef includes pseudoknot structure, thus we use vsfold5 for secondary structure prediction that we designed IRES IIIef construct, and we prepare two constructs IIIef 1a (52 nt) and IIIef 2b (91 nt). Preliminary analysis of the NMR spectrum of IIIef 1a RNA indicated that the construct tightly folded in solution and can be used for further structural analysis. The structural determinations of IIIef 1a and IIIef 2b are in progress with segmental as well as selective isotope labelling. It has been reported that formation of the IRES pseudoknot requires Mg^{2+} and, thus, the conformational change of IRES upon addition of Mg^{2+} will be analyzed by using RDC information.

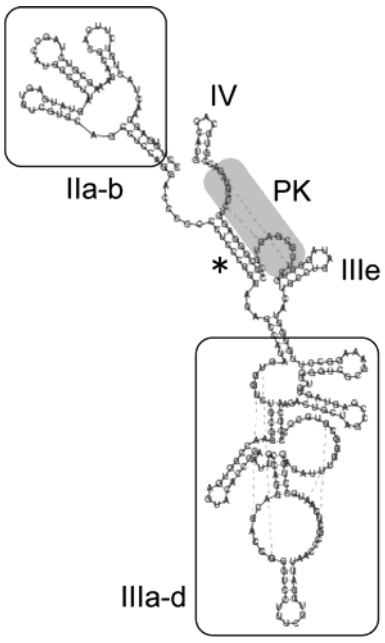

Fig. 3 Predicted secondary structure of HCV IRES by vsfold5

REFERENCES

1) Nakamura, S. (2009) *J. Biochem.* **146**, 251-261.
2) Dawson, W., Fujiwara, K., Kawai, G. (2007) *PLoS ONE* **2**, e905.

P-045 Two Natively Folded Conformations of Folate-bound Form of *E.coli* DHFR-D27E Mutant: NMR Signal Assignment and Structural Analysis

Tomoko Kunihara[1], Soichiro Kitazawa[1], Naohiro Kobayashi[2], Eiji Ohmae[3] and Ryo Kitahara[1]

[1]College of Pharmaceutical Sciences, Ritsumeikan University [2]Protein Research Institute of Osaka University [3]Department of Mathematical and life Science, Hiroshima University

Conformational fluctuations among the basic folded state and high Gibbs-free energy states have been recognized to be important for protein function, especially in enzymatic reaction. Dihydrofolate reductase (DHFR), which catalyzes the reduction of dihydrofolate to tetrahydrofolate, assumes a variety of conformations in solution. Our previous high pressure NMR study demonstrated that several cross-peaks in the $^{15}N/^{1}H$ HSQC spectrum are split into two with increasing pressure, thus we considered that the folate-bound form of *E.Coli* DHFR has two natively folded conformations in solution. Here, we show characterizations in structure and dynamics of the two natively folded conformations of the protein by using the DHFR mutant D27E that would favor the population of the minor conformer of the protein at physiological temperature and pressure. In D27E mutant, peak split is observed for amide protons, nitrogens and carbonyl carbons for several residues located at hinges of the M20 loop, FG loop, α_F-helix and GH loop, and peak intensity indicates that the mutant protein has about 30 % population of the minor conformer. ^{1}H, ^{15}N and ^{13}C chemical shifts indicate that the two conformers have closely similar backbone conformation. Moreover, the ^{15}N-R_1 and NOE analysis show that rapid segmental motions of the backbone in the ps-ns range are similar at two conformations. In contrast, large R_2 values are observed for many residues at the M20 loop, FG loop, GH loop and folate and NADPH binding regions. The split and broadening of the peaks appear to show a presence of slow conformational exchange between two conformations. The D27E mutant is suitable for direct detection of the minor conformer of the folate-bound DHFR, allowing further investigation of structure, dynamics and function of the protein.

High Gibbs-free energy conformers, including open conformer in enzyme and partially folded conformer, are key elements of protein structure that could be crucially important for function. The high-energy conformers are characterized usually by extremely low populations under physiological condition, rarely allowing for direct detection by NMR spectroscopy. We have demonstrated that pressure can cause a shift in population among the ensemble of conformers of a protein from folded to totally unfolded conformers. DHFR has a variety of conformations in crystals, depending on whether it binds the substrate, cofactor, or both. These conformations are classified into three major conformations, open, closed, and occluded. By using the high pressure NMR spectroscopy (1), we previously found two natively folded conformers in wild type (WT) of the folate bound *E. coli* DHFR in solution. However, structure and dynamics as well as its functional importance are largely

DHFR, conformational fluctuation, pressure, CLEANEX, R_2

unexplored. By using the DHFR mutant D27E, we demonstrate characterization in structure and dynamics of the two natively folded conformers of the protein.

NMR experiments were performed at 298 K on a DRX-600 spectrometer. In order to assign all backbone atoms of $^{15}N/^{13}C$ uniformly labeled D27E protein, triple resonance experiments were carried out. Secondary structure and order parameters were analyzed by the program TALOS. ^{15}N relaxation parameters, R_1, R_2 and heteronuclear NOE were obtained and Phase-modulated clean chemical exchange (CLEANEX-PM) NMR experiments were carried out for WT and D27E proteins.

We have assigned for the HSQC cross-peaks for 140 of 159 residues of the mutant. Moreover, 21 minor peaks were assigned to the residues located at hinges of the M20 loop, FG loop, α_F-helix and GH loop. Peak intensity indicates that the minor conformer is highly populated in the mutant sample. Interestingly, chemical shift differences between the split peaks corresponding to the major and minor conformations are remarkable for amide protons, amide nitrogens and carbonyl carbons. These observations indicate that hydrogen bond length and backbone torsion angles could be a major difference between the two conformations. Large R_2 values are observed for many residues at the M20 loop, FG loop, GH loop and folate and NADPH binding regions. The split and broadening of the peaks appear to show a presence of slow conformational exchange between the two conformations. The D27E mutant is suitable for direct detection of the minor conformer of DHFR, allowing further investigation of structure, dynamics and function of the protein.

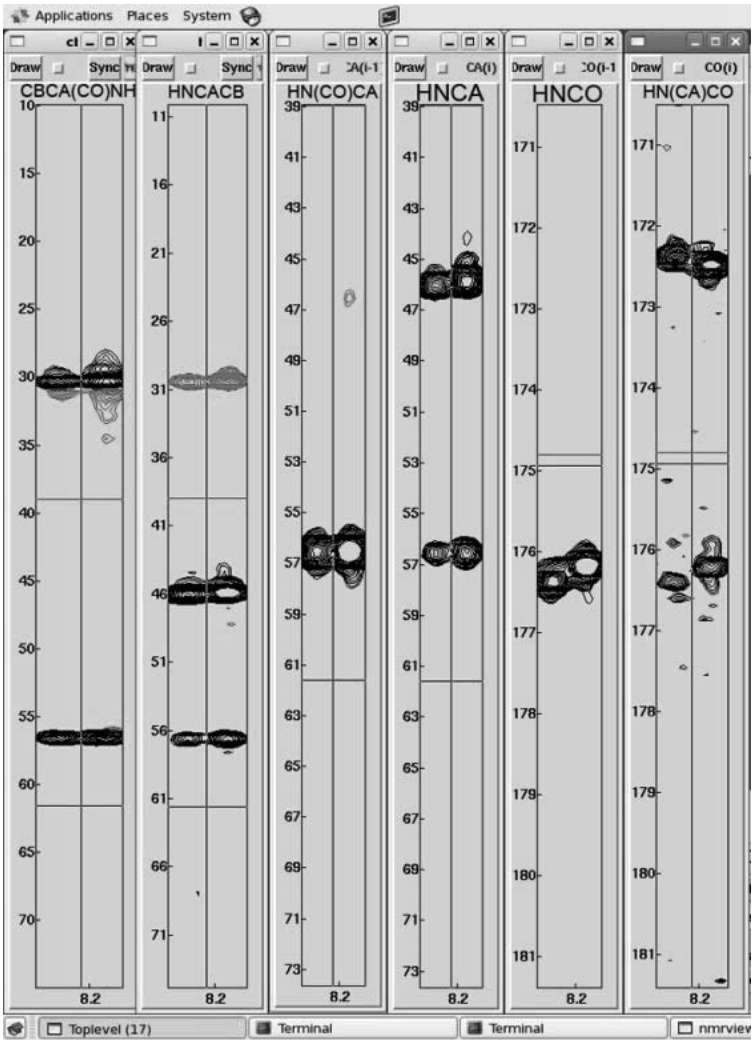

Figure 1. Slice spectra of CBCA(CO)NH, HNCACB, HN(CO)CA, HNCA, HNCO and HN(CA)CO. Peak split for G121 of D27E-DHFR.

Reference

1. Ryo Kitahara, Sina Sareth, Hiroaki Yamada, Eiji Ohmae, Kunihiko Gekko and Kazuyuki Akasaka (2000), *Biochemistry* **39**,12789-12795.

P-046 Structural and dynamical studies of transcriptional corepressor SHARP/SMRT complex

Ayaho Kobayashi[1], Suzuka Mikami[2], Teppei Kanaba[2], Yutaka Ito[2], Masaki Mishima[2]
[1]Department of chemistry, [2]Graduate school of science and engineering, Tokyo Metropolitan University

SHARP is known as a component of transcriptional repressor complexes functions in nuclear receptor and Notch signaling pathways. SPOC domain of SHARP binds to the C terminus of corepressor SMRT. We have determined the solution structure of the SPOC/phosphorylated SMRT. Interestingly, we found that unphosphorylated SMRT also binds to SPOC domain with weak affinity and the complex structure may be almost identical to phosphorylated stable complex deduced from NMR observation. For understanding the mechanism underlying the interaction, we have measured SPR and R2 dispersion to elucidate dynamics. Furthermore, we will discuss usage of paramagnetic relaxation enhancement (PRE) and lanthanide-binding tags (LBT) incorporated into β-turn to measure pseudo contact shifts (PCS) for obtaining the structural information in the weak interaction.

Introduction

SHARP, a transcriptional repressor, consists of two RNA binding domains (RRMs) and a transcriptional repressor binding domain SPOC. It is known as a component of transcriptional repressor complex that negatively regulates 17β-estradiol signaling pathway and Notch signaling pathways. We revealed that the SPOC domain of SHARP binds to phosphorylated C terminus of corepressor SMRT. In addition, SHARP also bind to unphosphorylated SMRT and forms weak complex. Comparison of NMR spectra suggested that structures of the stable (phosphorylated) complex and the weak (unphosphorylated) complex are almost identical. We are investigating how phosphorylation raises the affinity without structural changes from unphosphorylated state. To approach this problem, our current subjects are followings.

(1)Dynamic study of the weak complex and stable complex

(2)Structure determination of the weak complex

Results and Discussion

【1. Detection of exchange and determination of exchange rates】

At first, we measured R2 dispersion profile of ligand free SPOC domain. We measured CT CPMG experiments[(1)] and analyzed profiles using MATLAB based GUARDD[(2)] and NESSY[(3)]. So far, no significant exchanges were found in ligand-free state. Currently, we are analyzing the exchange of weak and stable complexes.

1. Tollinger, M., *et al*. *J. Am. Chem. Soc* (2001) 123, 11341
2. Kleckner, I. R., & Foster, M. P. GUARDD (http://code.google.com/p/guardd/)
3. Bieri, M. & Gooley, P., NESSY (http://home.gna.org/nessy/)
4. Barthelmes K., *et al*. (2011) *J. Am. Chem. Soc* 133, 808

Key words ; SHARP, R2-dispersion, PCS

【2. Structure determination of SPOC/unphosphorylated SMRT (weak complex)】

Comparison between HSQC spectra of the weak and stable complexes implied that both complex structures were almost identical. However, confirmation using more concrete structural evidence is required. Most straightforward confirmation is to determine the structure of the weak complex, but this may be hampered by missing the intermolecular NOEs due to exchange. To overcome this problem, we used followings methods.

(1) PRE

We introduced spin label (PROXYL) using single CYS mutants of SPOC domain. We also prepared the spin labeled SMRT peptide. We are currently investigating the weak complex structure using PRE.

(2) LBT incorporated into β-turn to measure PCS

Lanthanide-binding tags (LBTs) are also valuable tool for investigation of protein structure without NOEs. We adopted an incorporation of LBT (GYIDTNNDGWIEGDELY) into β-turn[(4)]. We inserted LBT into N3616-S3619 and succeeded in the measurement of PCS. However, many peaks were broadened. Thus, we are optimizing the samples.

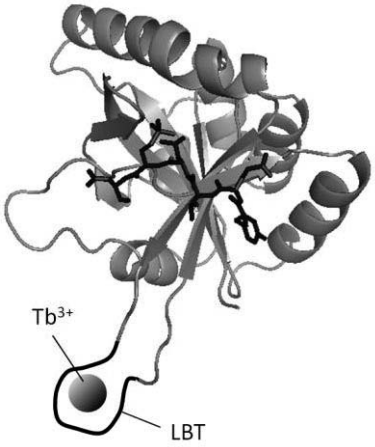

Ribbon drawing of LBT inserted SPOC domain

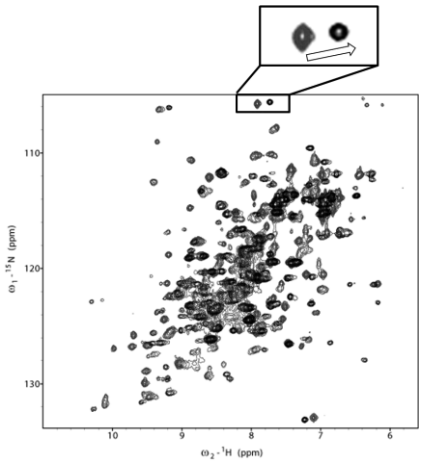

Observed PCS (La^{3+} and Tb^{3+}, gray and black respectively)

(3)SPOC-SMRT chimera

Genetically fused SPOC-SMRT may be useful to determine the unphosphorylated structure. In chimera, exchange is expected to be reduced by a linker, and intermolecular NOEs may be observed. We are currently optimizing the linker.

Perspective

We will reports exchange expected to exist in the weak and stable complex. We are also performing extensive SPR studies and will report binding kinetics analysed by R2 dispersion in combination with SPR analysis.

We also discuss determination of the complex structure of SPOC/unphosphorylated SMRT using PRE, PCS and preparation of chimera of SPOC domain with SMRT. Together, we will discuss the mechanism underlying the interaction between SPOC and SMRT.

P-047 Autoinhibition and activation of end-binding 1 revealed by NMR

Teppei Kanaba[1], Tomoyuki Mori[2], Ryoko Maesaki[2], Yutaka Ito[1], Toshio Hakoshima[2] and Masaki Mishima[1]
[1]Graduate School of Science and Engineering, Tokyo Metropolitan University
[2]Graduate School of Biological Sciences, Nara Institute of Science and Technology

End-binding 1 (EB1) is a member of plus end tracking proteins (+TIPs) which bind to microtubule (MT) plus end and regulate MT dynamics. EB1 binds to MT lattice with its N-terminal CH domain and stabilized MT. EB1 is thought to be autoinhibited by the interaction between CH domain and C-terminal domain. Despite the importance of the EB1–MT interaction in regulation of MT dynamics, the molecular details of the EB1 autoinhibition remain unclear.

We have attempted to reveal the molecular basis of the autoinhibition mechanism of EB1 using NMR spectroscopy. We identified the binding interface of CH domain with polymerized tubulin by transferred-cross saturation (TCS) experiments. In addition, by chemical shift perturbation (CSP) experiments, we identified the binding interface between EB1 CH domain and C-terminal domain. Our chemical shift perturbation experiments suggest that CH domain binds to C-terminal domain competitively with other target proteins. From these results, we will discuss molecular mechanisms of EB1 autoinhibition and activation.

RESULTS AND DISCUSSION

NMR spectra of full length EB1, EB1 CH domain and C-terminal domain

NMR spectra of full length EB1 (1-268), EB1 CH domain (1-130) and C-terminal (189-268) domain were measured (Fig. 1ABC) and the backbone resonances of CH domain and C-terminal domain were assigned. Using standard multi-dimensional NMR techniques, we established backbone resonance assignments of CH domain and C-terminal domain.

The chemical shifts of HSQC spectrum of CH domain were almost conserved in full length EB1. This suggests that the interaction between CH domain and C-terminal domain is weak or transiently, and there is no significant structural change in each domain.

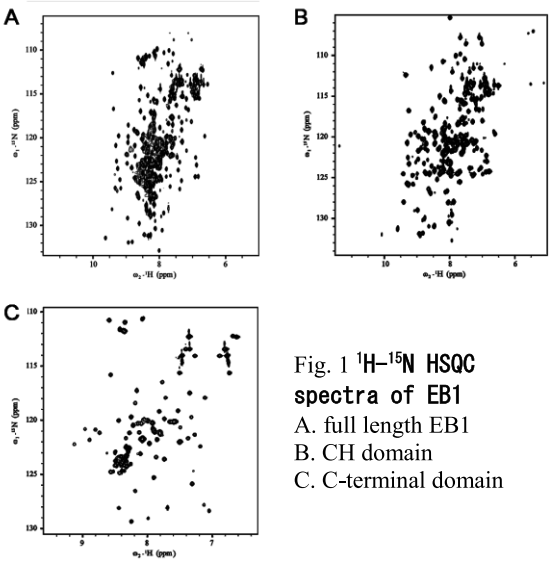

Fig. 1 ^{1}H–^{15}N HSQC spectra of EB1
A. full length EB1
B. CH domain
C. C-terminal domain

[REFERENCE]
(1) Takahashi, H., *et al*. (2000) Nat. Struct. Biol. 1,53-58
(2) Kanaba, T., *et al* (2010) The 49th Annual Meeting of The NMR Society of Japan, P031
(3) Hayashi I and Ikura M (2003) J. Biol. Chem 278, 36430-4 (4) Slep KC., *et al.* (2005) J Cell Biol. 168, 587-98
(5) Honnappa S., *et al.* (2009) Cell 138, 366-76 (6) Honnappa S., *et al.* (2006) Mol Cell. 23, 663-71.
(7) Nakamura M., *et al.* (2003) Curr. Biol. 11, 1062-7 (8) Hayashi I., *et al.* (2005) Mol Cell 19, 449-60

EB1, microtubule, transferred-cross saturation

The transferred-cross saturation experiment

To identify the binding interface of CH domain for MT, we applied TCS experiment[1] to this system. Our TCS experiments identified the binding interface of CH domain with polymelized tubulin[2]. At present, for more detail analysis, we construct CH mutants that interact with polymerized tubulin more weakly and will conduct TCS experiment more clearly.

The interaction site of CH domain with C-terminal domain

We performed CSP experiments of EB1 CH domain with C-terminal domain and investigated the relationship between CH domain - tubulin interaction and CH domain - C-terminal domain interaction. Since it was predicted that the interaction between CH domain and C-terminal domain was weak, we titrated ^{15}N-labeled CH domain with excess amounts of non-labeled C-terminal domain (CH domain : C-terminal domain = 1:5) in CSP experiment. As a result, line broadening of a number of peaks was occurred (Fig. 2AB). The C-terminal domain binding site was mapped for the crystal structure of CH domain[3] (Fig. 2C). By CSP experiments, we revealed that CH domain interacts with C-terminal domain by the same molecular surface of the binding interface of tubulin. These results indicate the autoinhibition is exerted by the masking of CH domain with C-terminal domain.

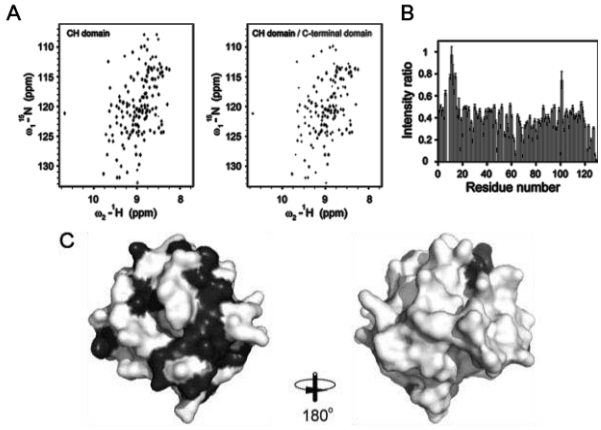

Fig. 2 **CSP experiments of CH domain**
A. HSQC spectra of CH domain in the absence (right) or presence (left) of C-terminal domain.
B. Signal intensity ratio.
C. Mapping of the affected residues (dark) on crystal structure of CH domain.

The interaction site of EB1 C-terminal domain with CH domain

We next investigated the interaction site of C-terminal domain with CH domain using CSP experiments. In CSP experiments, the signal intensity reduction was observed (Fig. 3AB) and the affected residues in the CSP experiments were mapped for the cystal structure of C-terminal domain[4] (Fig. 3C). Our CSP experiments revealed that CH domain interacts with C-terminal domain FYF motif, which is the central site of interaction with SxIP motif of APC or MACF2[5] and p150^{glued} CAP-Gly domain[6]. It is known that these target proteins activate the MT binding activity of EB1[7][8].

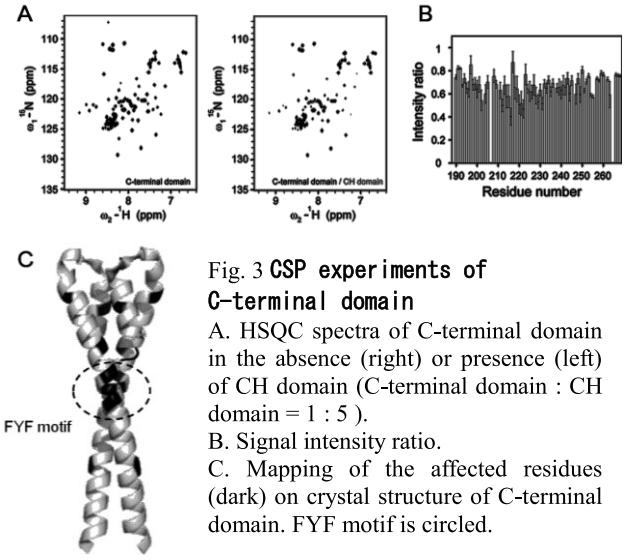

Fig. 3 **CSP experiments of C-terminal domain**
A. HSQC spectra of C-terminal domain in the absence (right) or presence (left) of CH domain (C-terminal domain : CH domain = 1 : 5).
B. Signal intensity ratio.
C. Mapping of the affected residues (dark) on crystal structure of C-terminal domain. FYF motif is circled.

Taken together these observations, we suggest that EB1 C-terminal domain inhibits the MT binding of CH domain by masking the interaction sites of CH domain for polymerized tubulin, and other target proteins bind competitively to FYF motif with CH domain. This target protein binding releases CH domain from C-terminal domain and released CH domain interacts with MT.

P-048 Structural study of ternary complex formation of IRF4 using NMR

Kouhei Sakaki[1], Katsutaka Akiyoshi[1], Yutaka Ito[1], Masaki Mishima[1]
[1]Department of chemistry, Graduated School of Science and Engineering, Tokyo Metropolitan University.

Structural determination of a multi-domain protein composed of flexible linkers and weak intra-interactions is hampered by technical difficulties, but it often contains interesting and important biological significance. IRF4 consists of two domains and forms higher order structure. IRF4 consists of N-terminal DNA binding domain and C-terminal regulatory domain which binds to phosphorylated PU.1. IRF4 and PU.1 form a complex on cognate DNA. We have prepared N-terminal region, C-terminal region and full length of IRF4, and PU.1. We obtained relatively dispersed TROSY spectrum of IRF4-full length. We will discuss reconstitution of IRF4-PU.1-DNA complex. Further, we also discuss collection of long-range distance information derived from PRE (paramagnetic relaxation enhancement) using spin labeling.

[**Introduction**]

IRF4 is known as a key transcriptional factor of B-cell proliferation and differentiation. IRF4 consists of N-terminal DNA binding domain and C-terminal regulatory domain. DNA binding ability of IRF4 is thought to be autoinhibited by C-terminal domain (Fig. 1). It is known that the C-terminal domain also binds to phosphorylated PU.1, and IRF4 and PU.1 form a complex on DNA (Fig. 1).

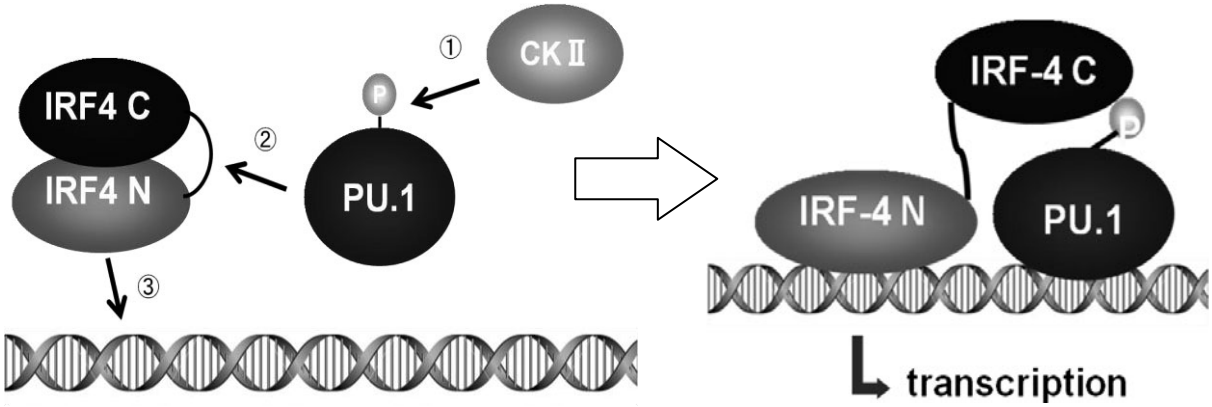

Fig.1 Schematic drawing of IRF4 interaction and its activation

[**Experiments**]

(1) Expression and purification of IRF4

We constructed several expression plasmids encoded full length, N-terminal domain, and C-terminal domain. We purified each domain, and ^{2}H (85%) and ^{15}N full-length IRF4 using Ni-NTA/GSH column and gel-filtration chromatography. We conducted NMR measurements of full-length, N-terminal domain, and C-terminal domain.

IRF4, ternary complex, multidomain protein

(2) Construction of PU.1,CKII co-expression system

We prepared plasmid that PU.1 fused to GST-tag. We inserted DNA sequence of CKII into the expression plasmid of PU.1 (pET49b) by infusion reaction (Fig. 2). We then confirmed protein expression in *E. coli* cell. We purified phosphorylated PU.1 by GSH sepharose column, following cleavage of GST-tag using HRV3C, re-pass of GSH column, and final separation using Phos-tag® Agarose (Wako).

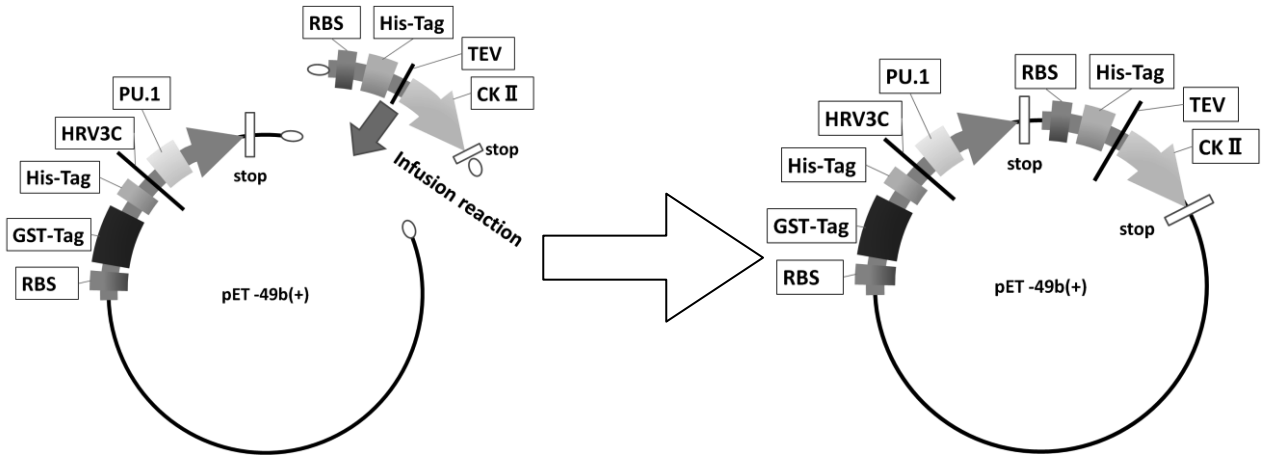

Fig.2 Preparation of PU.1 and CKII co-expression system

[Results and Discussion]

(1) IRF4

We obtained enough amount of purified full-length IRF4. ^{1}H-^{15}N TROSY showed relatively dispersed signals (Fig.1). In comparison with NMR spectra of N-terminal and C-terminal, it was interesting that the signals corresponds to C-terminal were broadened.

(2)Co-expression of PU.1 with CKII

We confirmed simultaneous expression of PU.1 and CKII in *E.coli* cell. We obtained enough quantity of phosphorylated PU.1 for measuring NMR by that purification system.

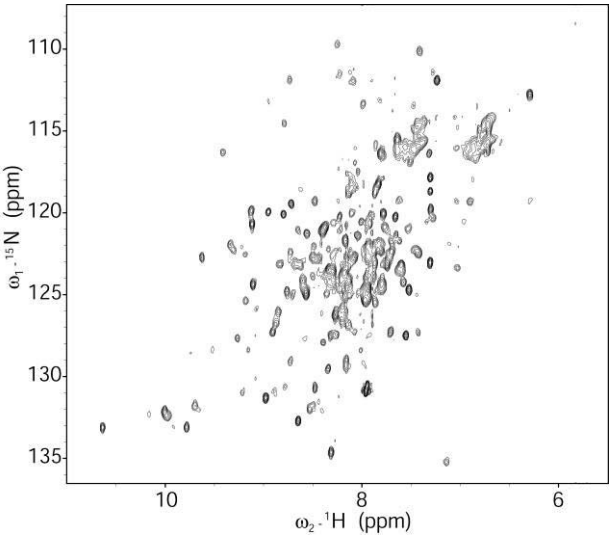

Fig.3 ^{1}H-^{15}N TROSY spectrum
^{2}H-^{15}N labeled full-length IRF4 (M.W. 52kDa)
50 mM Tris-HCl (pH 8.0), 400 mM KCl,
0.5 mM DTT and 0.1 mM EDTA

[Perspective]

We have prepared N-terminal domain, C-terminal domain. Further, we will discuss structure by using PRE (paramagnetic relaxation enhancement) by introducing spin label into C-terminal or N-terminal. Then, will discuss collect long-range distance information.

We finally construct IRF4/PU.1/DNA ternary complex. Our goal is structure determination of the ternary complex using NMR with variety of structural information such as PRE, PCS and RDC.

P-049 An attempt to obtain the structural insight of the multidomain protein PKC by solution NMR

Katsutaka Akiyoshi[1], Kensuke Miyazaki[1], Teppei Kanaba[1], Ryoko Maesaki[2], Yutaka Ito[1] and Masaki Mishima[1]
[1]Graduate School of Science and Engineering Tokyo Metropolitan Univesity
[2]Graduate School of Bioscience NAIST

Structural determination of a multidomain protein composed of inter-domain flexible linkers and weak intra interactions is an interesting issue but it is technically difficult. Protein kinase C alpha (PKCα), a multidomain protein, locates at cytoplasm in auto-inhibited state by inter domain interactions. When PKCα is activated by second messengers, Ca^{2+} and diacylglycerol (DAG), it is believed that a large conformation change occurs and it localizes at plasma membrane, and thus phosphorylates cognate substrates. As a first step of obtaining structural information of PKCα, we have prepared each domain. We aim to reconstitute full length PKCα by ligation reaction. We will also discuss usage of PRE derived from spin labeling to obtain long-range distance information in the meeting.

【Introduction】

Multidomain proteins play pivotal roles in many important phenomena in eukaryotes. To understand their functions, it is essential to analyze their structures. However, structural studies are hampered possibly due to weak domain-domain interaction and flexibility of linkers.

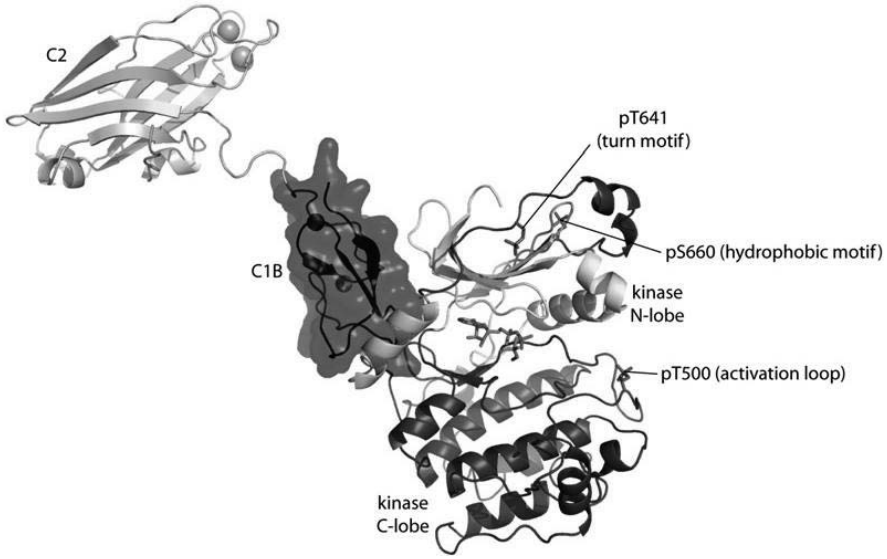

Fig.1 4.0Å Crystal structure of PKCβII
(Thomas A.L. et.al,Cell,144:55-66, 2011)

Our target for this study is Protein kinase C α (PKCα). It is believed that a conformation change occurs and PKCα localizes at plasma membrane when it is activated by second messengers, Ca^{2+} and diacylglycerol (DAG). PKCα is comprised of regulatory region and catalytic region. In the regulatory region, there are two tandem C1 domains, C1A and C1B (DAG binding domain) and C2 domain (Ca^{2+} binding domain).

Very recently, the full-length crystal structure of PKCβII has been reported (Fig.1). However, the domain arrangement and the interaction between the domains are still elusive. In fact, electron density of C1A domain was missing and C2 domain was flipped out due to crystal packing.

Multidomain protein, PRE, Protein kinase C

【Strategy】

(1)Purify each domain.

(2)Reconstruct full-length PKCα by ligation of each domain.

(3)Determine its structure by acquisition of structural information from PRE.

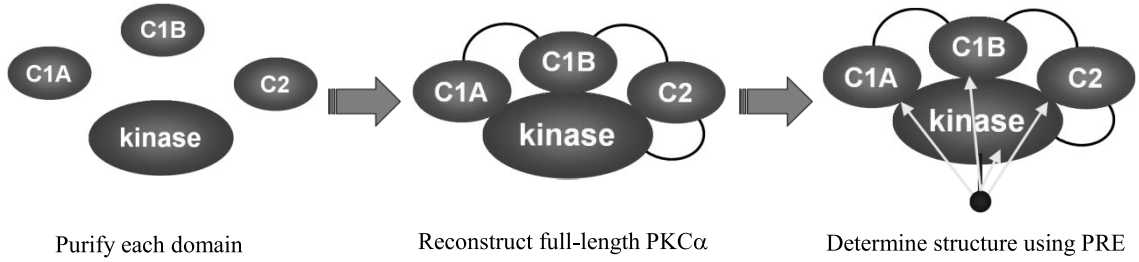

Fig. 2 Strategy of this study

【Results and Discussion】

As a first step, we investigated domain interactions between C1B and C2 domain. We measured 2D ^{1}H-^{15}N HSQC spectra of tandem C1B-C2 region of PKCα to verify the interaction between C1B and C2 domain (Fig.3a). Comparison with ^{1}H-^{15}N HSQC spectrum of C1B is shown in Fig.3b. The chemical shift of C1B domain was slightly different between the two spectra. This result suggests that there is an interaction between C1B and C2 domain in solution.

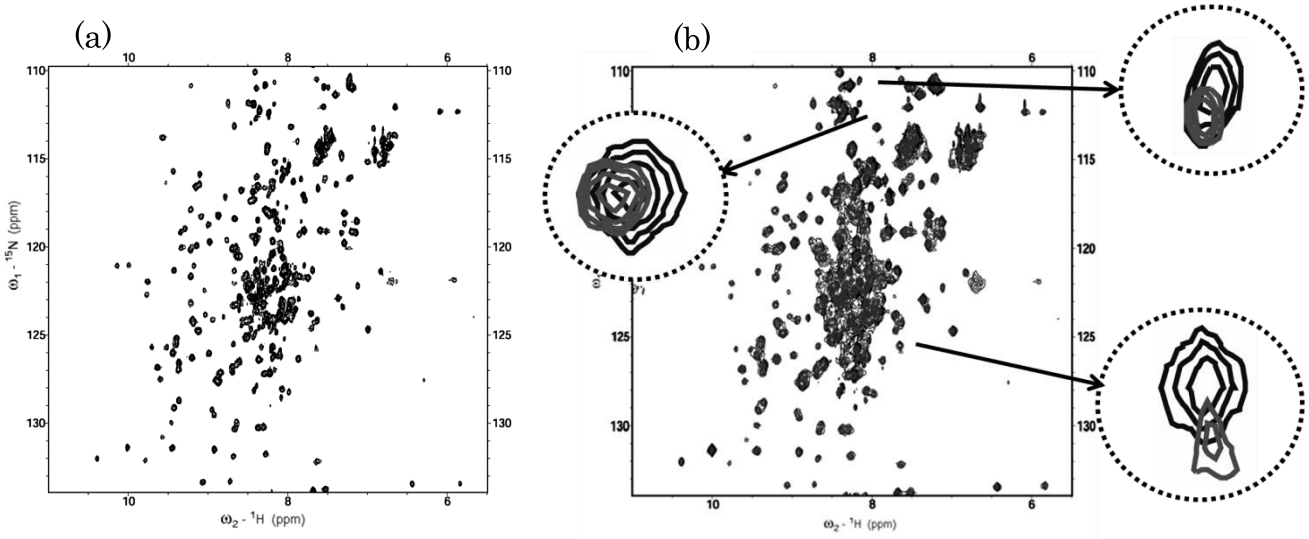

Fig.3 ^{1}H-^{15}N HSQC spectra

(a) spectrum of C1B-C2 domain, 0.05 mM, 50 mM MES (pH 5.5), 50 mM KCl, 303 K

(b) spectrum of C1B and C1B-C2 domain, 0.05 mM, 50 mM MES (pH 5.5), 50 mM KCl, 303 K

【Perspectives】

Currently, we are trying to construct the expression system of kinase domain and to purify C1A domain. In this meeting, we would like to discuss reconstitution of full-length PKCα or several domains of PKCα by ligation. We also would like to discuss acquisition of long-range distance information using PRE.

P-050

NMR analysis of an oligosaccharyltransferase that catalyzes the Asn-linked glycosylation

James Nyirenda, Shunsuke Matsumoto, Takashi Saitoh, and Daisuke Kohda

Medical Institute of Bioregulation, Kyushu University

Asparagine-linked (N-) glycosylation of proteins is a widespread not only in eukaryotes but also in archaea and some eubacteria. Oligosaccharyltransferase (OST) creates the oligosaccharide-asparagine linkage by transferring glycan from a lipid-linked oligosaccharide donor to the asparagine residue in the selected N-glycosylation sequons (N-x-T/S; x≠P). The catalytic subunit is STT3 in eukaryotes, AglB in archaea, and PglB in eubacteria. STT3/AglB/PglB consists of an N-terminal multi-span transmembrane domain and a C-terminal globular domain. The C-terminal globular domain contains a well-conserved, five-residue motif, WWDYG, which constitutes the +2 Thr/Ser-recognizing pocket.

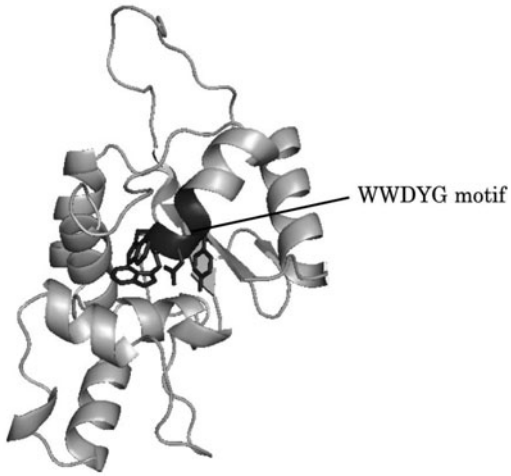

Fig.1 X-ray crystal structure of the C-terminal globular domain of OST from *Archaeoglobus fulgidus* (*Af*AglB-S2)

The comparison of the crystal structures of the C-terminal globular domains of AglB from *Pyrococcus furiosus* and PglB from *Campylobacter jejuni* revealed a large conformational variation of the WWDYG motif, raising a question about what the true conformation of the segment without crystal packing effects would be. To answer this question, we selected two close AglBs from *Pyrococcus horikoshii* and *Pyrococcus abyssi*, and two distant AglBs from *Archaeoglobus fulgidus,* and determined their crystal structures. The sequence identity of the two *Pyrococcus* AglBs is about 70%, and that of the two *Archaeoglobus* AglBs is about 30% to *P. furiosus* AglB, respectively. We then performed a holistic comparison of the six structures with emphasis on the conformation of the WWDYG motif. We found a highly superimposable pair: one of the *A. fulgidus* AglB, referred to as S2, and *C. jejuni* PglB, even with sequence identity less than 30%. We proposed that this pair represented the conformation of the resting state of OST. In the present study, we investigated the molecular motions of the C-terminal globular domains by the NMR relaxation analysis.

The *A. fulgidus* genome contains three AglB paralogs, named *Af*AglB-L (868 amino acid residues), *Af*AglB-S1 (591 amino acid residues), and *Af*AglB-S2 (593 amino acid residues). Good quality NMR spectra were obtained for the C-terminal globular domain (residues 433-593) of *Af*AglB-S2 in 20 mM MOPS-NaOH pH7.0 at 308K. The 91% of the ^{15}N and ^{1}H backbone signals were assigned using 3D HNCOCACB, CBCACONH, HNCO, and HNCACO spectra of a uniformly ^{13}C/^{15}N-labeled protein, and 2D ^{1}H-^{15}N HSQC spectra of ^{15}N-isotopic labeling selective

for Tyr, Try, Lys, or Ala. The NH signals of 14 amino acid residues located on loop regions were missing on the ^{1}H-^{15}N HSQC spectrum.

We carried out ^{15}N relaxation experiments using uniformly ^{15}N-labeled *Af*AglB-S2 to investigate the molecular motions for each time scale. The results of ^{15}N relaxation experiments (heteronuclear NOE, R_1, and R_2) were shown in Fig. 2. In the heteronuclear NOE experiment, low values (noe < 0.6) were observed at some amino acid residues on the loop regions in the crystal structure. The large R_2 values were observed for the WWDYG motif residues and the following α-helical and loop structures. These large R_2 values ($R_2 > 20$ s^{-1}) were assumed to contain a R_{ex} term caused by conformational changes in millisecond to sub-millisecond time scales.

At present, we have prepared an *Af*AglB-S2 mutant containing a specially designed disulfide bond to fix the motions in the flexible region. The incorporation of the corresponding disulfide bond in the full-length *Pyrococcus furiosus* AglB reduced the OST activity substantially. The assignment of the ^{15}N and ^{1}H backbone signals and ^{15}N relaxation experiments are now in progress.

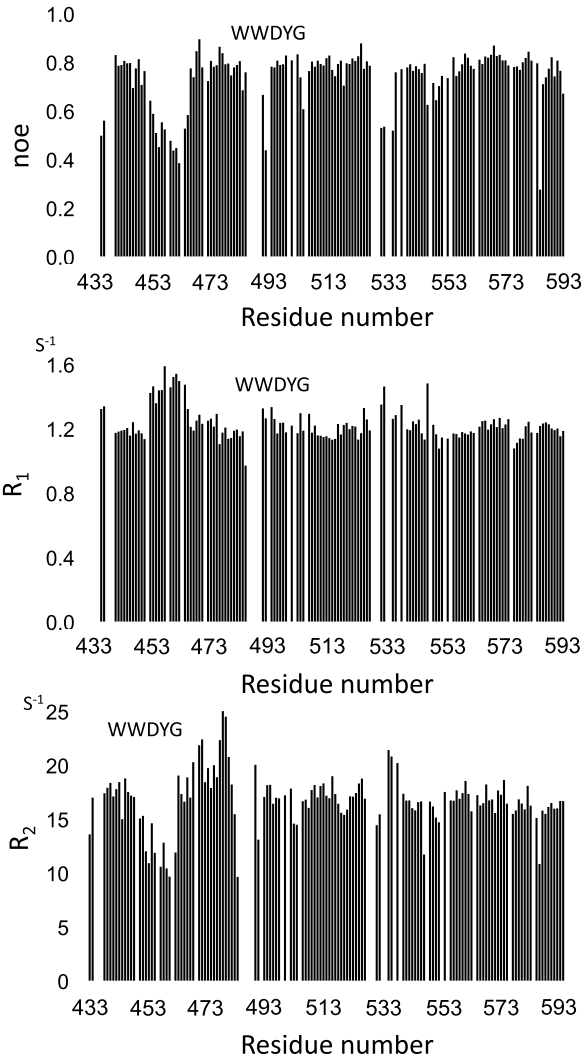

Fig.2 ^{15}N relaxation analysis of C-terminal globular domain of *Af* OST S2

P-051 NMR study on the basic domain of telomeric protein TRF2 bound to Holliday junction

Yoshinao Iwasawa[1], Hideaki Shimojo[1] , Motoki Murai[1] , Ryo Kanno[1] and Yoshifumi Nishimura[1]

[1]Department of Supramolecular Biology, Graduate school of Nanobioscience, Yokohama City University (Japan)

ABSTRACT

Telomeres are specific structures at the end of chromosomes and are essential for maintaining genome stability and cell viability. The human telomeric protein TRF2 plays a role in the maintenance and the protection of telomeres, and takes part in the formation of t-loop. TRF2 contains basic domain, dimerization domain and DNA-binding domain. The basic domain is reported to interact with Holliday junction. Here, we will clarify the interaction mode of TRF2 basic domain and Holliday junction by NMR.

[Introduction]

The region of DNA that shortens at the cell division of telomere exists in the end of the eukaryotic chromosome, and this telomere is assumed to be related to the cell senescence and cancer. A lot of proteins involved in telomere protection and maintenance are often known. TRF1 and TRF2 are related to the composition of the t-loop structure of the telomere end part. TRF2 has the maintenance of the telomere besides the formation of t-loop and the function to protect. Especially, the report that the basic domain is interactive with the stabilization of t-loop, the stabilization of the Holliday Junction, and telomeric G-quadruplex structures is done. In this study, we intend to clarify the details of the interaction of TRF2 basic domain(TRF2basic) and Holliday Junction by NMR.

[Experiment]

●Purification of TRF2basic

The refinement of TRF2basic cultured in large quantities by using the E. coli bacteria of the TRF2basic expression system, added IPTG, and did the induced expression. Then, we purified TRF2basic monomer via affinity chromatography, and HPLC. For dimerization of the TRF2basic, oxidized monomers using air pump. The collected samples were purified through HPLC. Then, TRF2basic dimer replaced the 10mM KPB buffer(pH6.8) to this sample. TRF2basic monomer replaced 10mM KPB buffer(pH6.8) added 10mM D-DTT.

●Purification of Holliday Junction

Mixing the DNA sequence of each DNA single strand 18mer have been reported to be purified Holliday junction(18HJ(fig.2)), annealing at 98℃, which was purified via HPLC. Then, 18HJ replaced the 10mM KPB buffer(pH6.8) .

We performed titration experiments that used those purified TRF2basic and 18HJ.

Telomere

[Result and Discussion]

●Titration experiments

In titration experiments with TRF2basic monomer and 18HJ, chemical shift change was observed Arg30, Leu35, Ala39, Glu40, Glu45 in the ^{1}H-^{15}N HSQC spectrum.(Fig.1) Thus, it appears that you are acting on the binding of the C-terminal basic region of TRF2basic monomer. We do not experiment a titration of TRF2basic dimer and 18HJ yet, so we will try that experiment. And, I think to seek a change in the chemical shift of the dissociation constants(Kd) from 1D spectra of iminoproton 18HJ.(Fig.3)

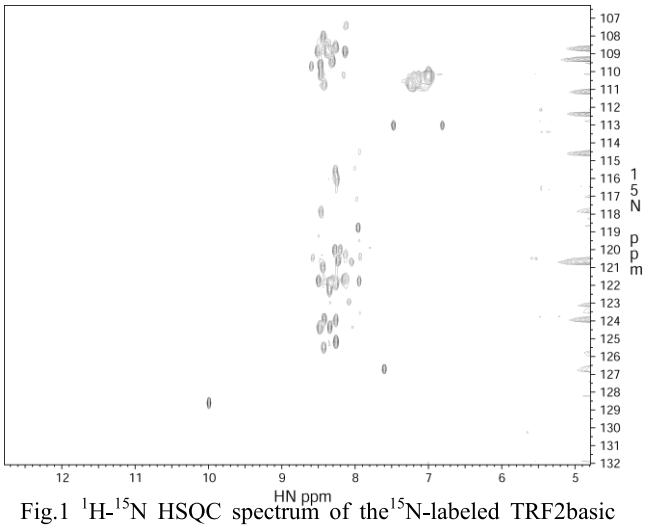

Fig.1 ^{1}H-^{15}N HSQC spectrum of the ^{15}N-labeled TRF2basic monomer/18HJ complex.

●Attribution of 18HJ

For titration experiments, we have to identify the interaction sites 18HJ, we have attributed the 18HJ from the NOESY spectrum signal of iminoproton. However, Only NOESY spectra of 18HJ is difficult to think of belonging. Then, double-stranded DNA in each arm of the same array of 18HJ, and purified the same as 18HJ. We have the attribution of each arm from the NOESY spectra were measured. The reference to the attribution of each arm, made the attribution of 18HJ.

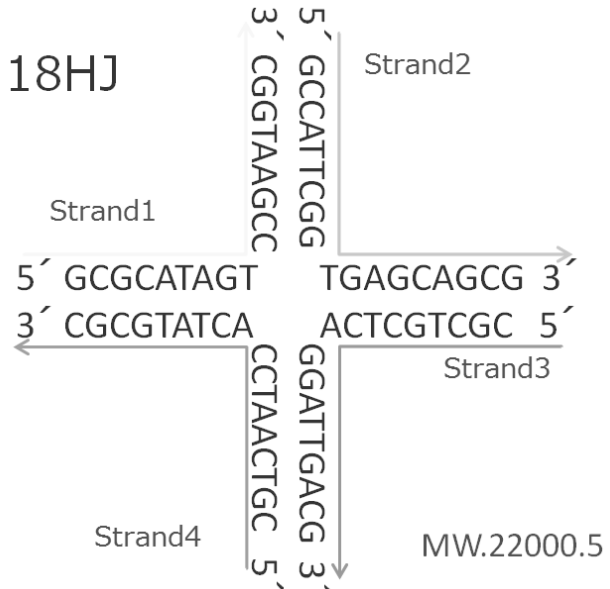

Fig.2 18HJ (J Biol Chem. 1996 Oct 18;271(42):26105-9. Analysis of substrate specificty of the RuvC holliday junction resolvase with synthetic Holliday junctions. Shida T et al.)

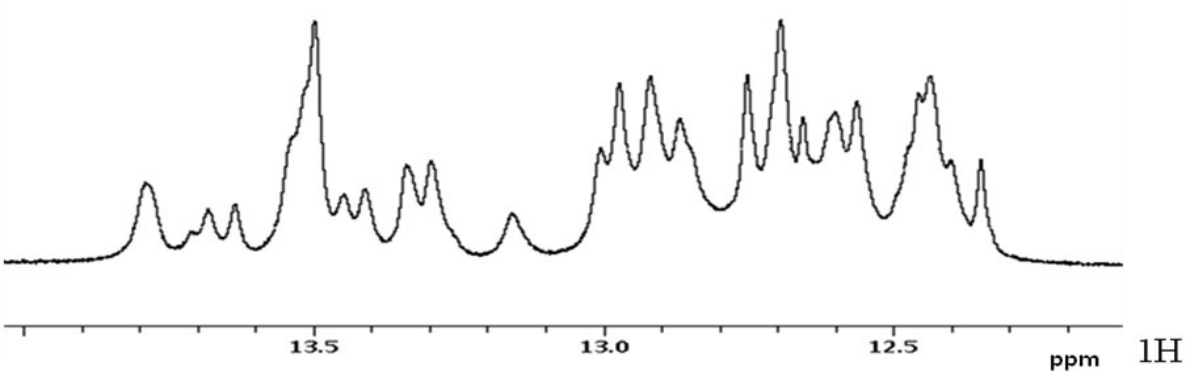

Fig.3 18HJ: 1D spectra of iminoproton / 18HJ free

P-052 The interaction analysis of CENP-S/X and CENP-T/W by NMR

Masahiro Takahashi[1], Aritaka Nagadoi[1], Tatsuya Nishino[2, 3], Tatsuo Fukagawa[2, 3], Yoshifumi Nishimura[1]
[1]Division of Structural Biology, Graduate School of Nanobioscience, Yokohama City University
[2] National Institute of Genetics
[3] The Graduate University for Advanced Studies

A lot of centromere proteins assemble and form the particular structure called kinetochore. At the basic part of the kinetochore, two centromere proteins T and W form a complex (CENP-T/W) which binds to centromere DNA and participates in the particular centromere chromatin structure. Then two other centromere proteins S and X forming a complex (CENP-S/X) bind to CENP-T/W. Here we have studied the interaction of CENP-S/X and CENP-T/W by NMR.

【Introduction】

The centromere is the thin part of two identical sister chromosomes connected. In cell division the microtubules bind to the centromere formed by the special three layer structure (kinetochore) consisting of a lot of kinetochore proteins. Then two sister chromosomes are divided into each sister cell.

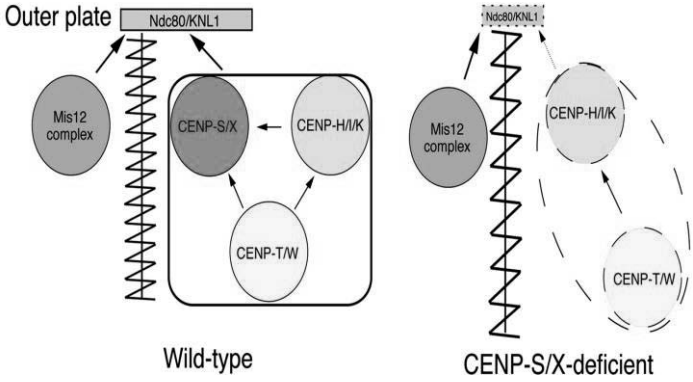

Fig.1. A model for the assembly of kinetochore protein at mitosis.

In the part of kinetochore, the CENP-T/W complex formed by two centromere proteins T and W binds to centromere DNA forming a peculiar centromere chromatin. Then CENP-S/X complex formed by two centromere proteins S and X binds to CENP-T/W. In the cell which lacks CENP-S/X, electron micrograph experiment showed that the length of the part of kinetochore outer plate was shorten and the distance between the outer plate and the centromere chromatin became long. In the cell which lacks CENP-T or CENP-W, the chromosome caused overcondensation and abnormal chromosome distribution was observed.

So CENP-S/X and CENP-T/W are interactive and important in the chromosome partitioning. However, the interaction mechanism between them is now well understood. Here, we will try to reveal the interaction mechanism of CENP-S/X and CENP-T/W by NMR.

centromere protein, interaction, kinetochore

【Experiment】

Each of the His-tagged CENP-S/X complex and the His-tagged CENP-T/W complex was expressed in a E.coli co-expression vector system. Each of the lysed supernatant was loaded onto the His-accept column chromatography. The His-tag was cut out by TEV protease. Then each sample was loaded onto the His-accept column again and loaded onto the gel filtration column chromatography.

【Results and Discussion】

The CENP-S/X and the CENP-T/W complexes were mixed and loaded onto the gel filtration column chromatography. The ternary complex formation between the CENP-S/X and CENP-T/W complexes was confirmed by the gel filtration column chromatography. Then we have measured 2D ^{1}H-^{15}N HSQC spectra of a ^{15}N-labeled CENP-S/X complex and of a ternary complex of CENP-S/X and CENP-T/W complexes that was obtained by mixing of ^{15}N-labeled CENP-S/X and non-labeled CENP-T/W. Both spectra are entirely different, so the structural change of the CENP-S/X complex by binding to the CENP-T/W complex was suggested.

Now, we have examined the solution conditions of NMR experiments so that all signals of target protein may appear to reveal the interaction mechanism between CENP-S/X and CENP-T/W.

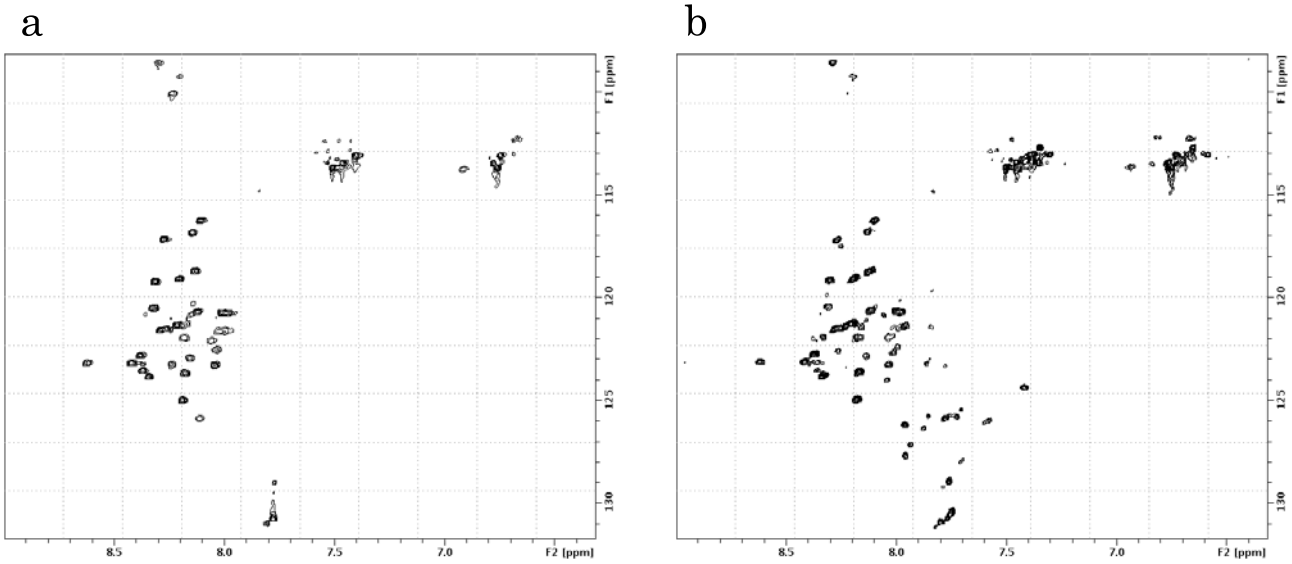

Fig.2. ^{1}H-^{15}N HSQC spectrum.
a. ^{15}N-labeled CENP-S/X.
b. ^{15}N-labeled CENP-S/X with CENP-T/W.

【References】

1) Miho Amano, Aussie Suzuki, Tetsuya Hori, Chelsea Backer, Katsuya Okawa, Iain M. Cheeseman,and Tatsuo Fukagawa. (2009) J.Cell Biol. Vol.186 No.2, 173 - 182.
2) T. Hori, M. Amano, A. Suzuki, C.B. Backer, J.P. Welburn, Y. Dong, B.F. McEwen, W.H. Shang, E. Suzuki, K. Okawa, I.M. Cheeseman and T. Fukagawa. (2008) Cell 135, 1039 - 1052.

P-053 Heteronuclear multidimensional NMR spectroscopy of proteins in human cultured cells

Kaori Onishi[1], Jumpei Hamatsu[1], Dambarudhar Shiba Sankar Hembram[1], Takahiro Haremaki[1], Teppei Ikeya[1], Masaki Mishima[1], Masahiro Shirakawa[2] and Yutaka Ito[1]
[1]Department of Chemistry, Tokyo Metropolitan University,
[2]Department of Molecular Engineering, Kyoto University

Abstract

In-cell NMR spectroscopy of human cultured cells will provide a powerful tool not only in biological but also in medical and pharmaceutical researches. However, the low intracellular concentration of target proteins makes it difficult to obtain 3D NMR spectra. Aiming at measuring 3D triple-resonance NMR spectra of proteins in human cultured cells, we have initiated methodological developments/optimisations in stable isotope labelling of target proteins, rapid measurement of multidimensional NMR spectra, improved data processing algorithms, etc. In this presentation, we report our recent progress in in-cell NMR studies of two model proteins, GB1 and TTHA1718, in living HeLa cells.

In-cell NMR spectroscopy [1] opened new avenues for the investigation of protein conformations at atomic resolution and how they change in response to biological events in living environments. This method has been successfully applied to proteins overexpressed in *Escherichia coli*, and we have reported the first 3D protein structure determined exclusively on the basis of information obtained in living cells [2,3]. Extending in-cell NMR to study proteins inside higher eukaryotic cells, and thus making this method more useful in medical and pharmaceutical researches, was another issue to be investigated. Inomata *et al.* introduced an innovative method that enables in-cell NMR in human cells by which the target protein is delivered into the cells by tagging it with a cell-penetrating peptide [4]. However, low intracellular concentration (20-30 μM) of proteins and limited measurement time (within a few hours) have so far prevented us to obtain high resolution 3D triple-resonance NMR spectra which are measured when resonance assignment and further analyses are required.

We have initiated modification and optimisation of existing in-cell NMR methods aimed at measuring 3D triple-resonance NMR spectra for backbone resonance assignment of proteins inside living cultured HeLa cells. In this presentation we report our recent in-HeLa cell NMR results on two model proteins, *Thermus thermophilus* HB8 TTHA1718 (66 residues) and *Streptococcus* protein G B1 domain (GB1, 57 residues).

The incorporation of TTHA1718 and GB1 into HeLa cells for in-cell NMR spectroscopy is carried out by using essentially identical protocols described previously [4]. Stable isotope-labelled TTHA1718 and GB1 proteins were produced in *E. coli* cells and purified. For both proteins, a

Key words: In-cell NMR, multidimensional NMR, Protein structure

C-terminal cyteine residue was introduced by site-directed mutagenesis, so as to be linked with chemically synthesised cell-penetrating peptides with disulphide bonds.

2D ^{1}H-^{15}N SOFAST-HMQC experiments of HeLa in-cell NMR samples showed well-resolved 2D spectra for both TTHA1718 and GB1, thus indicating that the incorporation into the cytosol of cultured cells was carried out successfully. For the indirectly acquired dimension nonlinear sampling scheme and maximum entropy processing were employed. Figure 1 shows the ^{1}H-^{15}N SOFAST-HMQC spectrum of TTHA1718 inside HeLa cells together with the ^{1}H-^{15}N HSQC spectrum of TTH1718 *in vitro*.

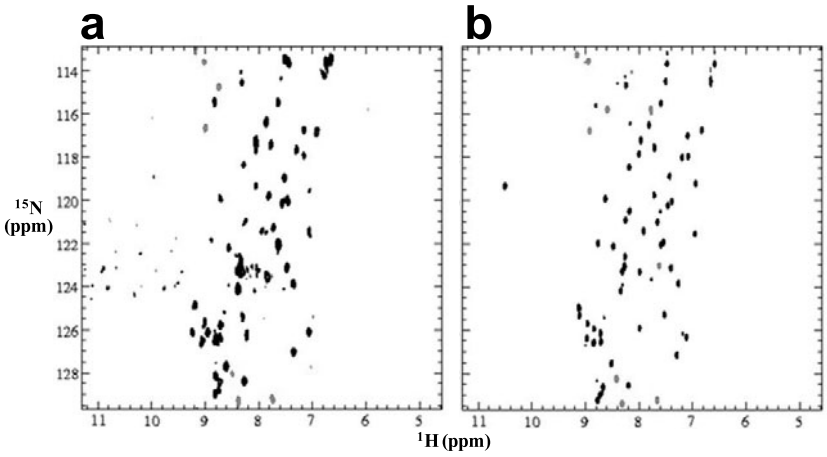

Figure 1
a. The 2D ^{1}H-^{15}N SOFAST-HMQC spectrum of TTHA1718 in HeLa cells. The indirectly acquired dimension (^{15}N) was measured with a nonlinear sampling scheme and processed with 1D maximum entropy using Azara v2.8 software (W. Boucher, www.bio.cam.ac.uk/azara). **b**. The 2D ^{1}H-^{15}N HSQC spectrum of TTHA1718 *in vitro*.

As was demonstrated in the 2D ^{1}H-^{15}N correlation spectra, band-selective excitation and short transient approach [5] seems to be very beneficial for in-cell NMR experiments, particularly for the case using cultured HeLa cells, where lower intracellular concentration of target proteins and short life time of the cell samples are the issue. With this approach it was reported that the time requirements for NMR experiments *in vitro* have been reduced from tens-of-minutes to seconds for 2D NMR experiments, and from days to hours (and even to minutes in combination with nonlinear sampling) in the case of 3D NMR experiments. As the next step, we are measuring the Band-selective Excitation Short-Transient (BEST) version of triple-resonance experiments [6] of TTHA1718 and GB1 inside HeLa cells. Considering much slower rotational tumbling of proteins due to higher viscosity inside cells, the sensitivity improvement by protein perdeuteration with TROSY-based approach will be tested.

References:

1. Serber, Z. et al. *J. Am. Chem. Soc.* **123**, 2446-2447 (2001).
2. Sakakibara, D. et al. *Nature* **458**, 102-105 (2009).
3. Ikeya, T. et al. *Nat. Protoc.* **5**, 1051-1060 (2010).
4. Inomata, K. et al. *Nature* **458**, 106-109 (2009).
5. Schanda, P., Kupce, E. & Brutscher, B. *J. Biomol. NMR* **33**, 199-211 (2005).
6. Lescop, E., Schanda, P. & Brutscher, B. *J. Magn. Reson.* **187**, 163-169 (2007).

P-054 Structural factors responsible for the regulation of the stability of Fe-Met coordination bond in cytochrome *c*

Shin-ichi Mikami, Yukie Izumoto, Hulin Tai, and Yasuhiko Yamamoto
Department of Chemistry, University of Tsukuba

ABSTRACT

Role of the unique hydrogen bonds formed between main chain of axial ligand Met59 and Gly50 in *Hydrogenobacter thermophilus* cytochrome c_{552} were characterized. In this study, we revealed that the Fe-Met coordination bond is considerably weakened by removing this unique main chain hydrogen bond network through G50P mutation. As a result, side chain of Lys residue replaces the side chain of Met59 and coordinates to heme Fe at high temperature in the G50P mutant. This finding indicated that the Gly50-Met59 hydrogen bond network is an important structural factor for the regulation of the Fe-Met coordination bond, and hence function of the protein.

INTRODUCTION

Hydrogenobacter thermophilus cytochrome c_{552} (HT) is an electron transfer protein consists of 80 amino acid residues and heme. Side chains of His14 and Met59 binds to heme Fe as axial ligands, and these ligands play significant roles on redox function and thermostability of the protein. Main chain amide NH and CO of Met59 are forming hydrogen bonds with CO and NH of Gly50, respectively, therefore these hydrogen bonds are expected to have some impact on thermostability of the coordination bond. In this study, we removed this hydrogen bond by replacing Gly50 with Pro, and investigated the effect of the mutation.

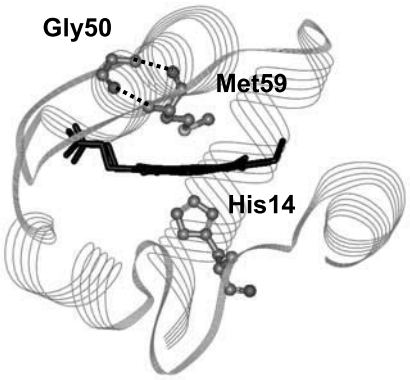

Fig. 1. Tertiary structure of the wild-type HT (PDB : 1YNR). The unique hydrogen bonds formed between G50 and M59 are shown.

RESULTS AND DISCUSSION

Effect of the mutation on thermostability of the protein.

Fe-Met coordination bond has characteristic absorption at 686 nm in its absorption spectra, thus plotting the absorbance at 686 nm against temperature would provide information about cleavage temperature (Tm_c) of the Fe-Met bond. Temperature dependence of absorption spectra of the G50P mutant is compared with that of wild-type HT in **Fig. 2**, and absorbance at 686 nm of two proteins are plotted against temperature. In the spectra of the G50P mutant, absorption observed at 686 nm gradually decays as temperature increase, while spectra of HT are almost unchanged over the temperature range examined. The Tm_c values of 64.8 ℃ and 100 ℃ > were obtained for the G50P mutant and wild-type HT, respectively. Also in the absorption spectra of the G50P mutant, a band derived from high-spin state formed as a result of the Fe-Met bond cleavage is observed around 625 nm in the low temperature range. This result indicated that the unique G50-M59 main chain hydrogen bond network contribute significantly to the stability of the Fe-Met bond.

We also compared temperature dependence of circular dichorism spectra of the G50P and HT proteins in order to estimate the effect of the mutation on thersmostability of the whole protein structure. Thermal denaturation temperature (Tm_α) was calculated from $\phi_{(222\ nm)}$ vs. temperature plots and the values of 105.0 ℃ and 109.8 ℃ were obtained for the G50P and HT proteins, respectively. Effect of the mutation on Tm_α value was smaller than the Tm_c one, therefore the unique hydrogen bond network was revealed to selectively increase the stability of Fe-Met coordination bond.

Keywords: Cytochrome *c*, Axial ligand, Hydrogen bond

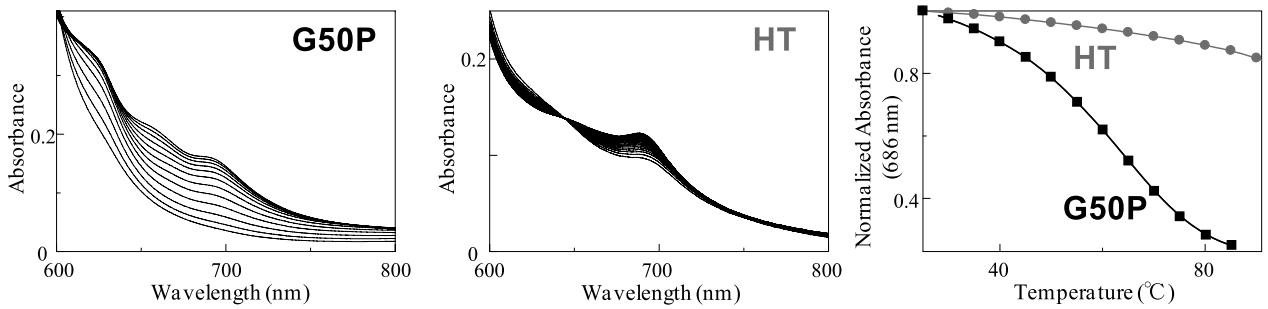

Fig. 2. Temperature dependence of absorption spectra of the oxidized G50P mutant (left) and the wild-type HT (center) at pH = 7.0. The plots of normalized absorbance at 686 nm against temperature are plotted at right (G50P ■, HT ●).

^{1}H NMR spectra of the G50P mutant and wild-type HT.

In order to probe the effect of the mutation on protein structure, ^{1}H NMR spectra of the G50P mutant were taken at various temperatures and compared with that of wild-type HT (**Fig. 3**). In the spectra of the G50P mutant, signal of Met59-$C_\varepsilon H_3$ observed at -17.9 ppm and heme methyl proton signals (16.7 ppm ~ 24.7 ppm) derived from Met59 coordinated form disappear at 57 ℃, while those signals of wild-type HT are almost unchanged in the spectra. After 57 ℃, set of heme methyl proton signals observed at 15.9 ppm ~ 22.8 ppm increase their intensities, indicating the replacement of axial Met59 with new axial ligand. This high temperature ligand was identified as Lys by measuring ^{1}H NMR spectra of the chemical modified G50P mutant (Data not shown here). In spectra of the G50P mutant, signals derived from high spin form are observed in the range of 41.0 ppm ~ 48.6 ppm at 25 ℃ along with the signals of Met and Lys coordinated form, which is consistent with the results from absorption spectra.

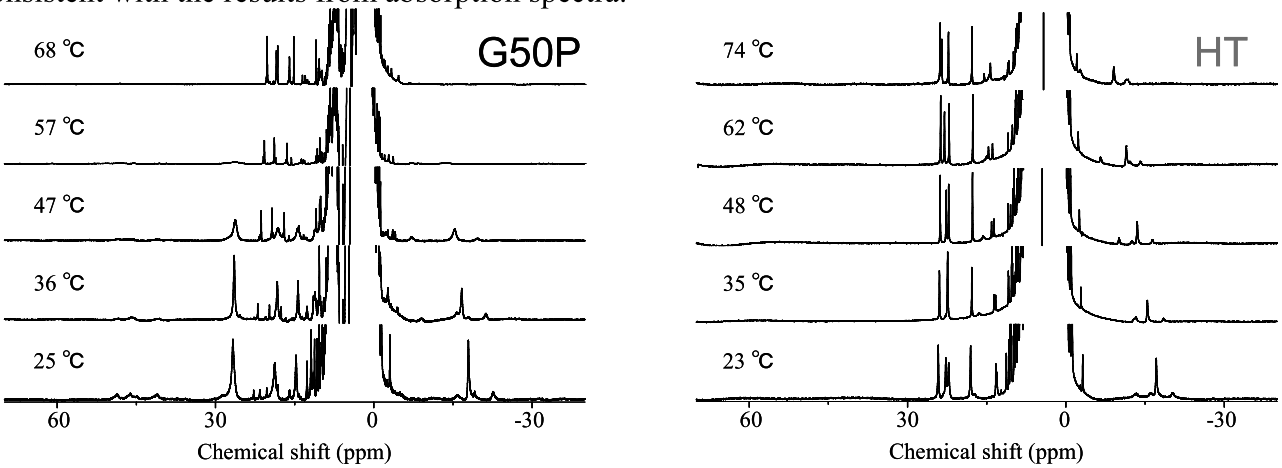

Fig. 3. ^{1}H NMR spectra of the oxidized G50P mutant (left) and wild-type HT (right) at pH = 7.0.

Redox function of the G50P mutant.

Redox function of cytochrome *c* is evaluated by redox potential, and the values of Met coordinated form, high spin form, and Lys coordinated form of the G50P mutant and wild-type HT at 25 ℃ are 247 mV, 20 mV, - 529 mV, and 245 mV, respectively. Redox potential of the G50P mutant is as same as that of wild-type HT when having same axial ligands set, but largely differs when having the different ligands sets, indicating importance of the axial ligands on redox function of the protein.

CONCLUSION

In this study, we revealed contribution of the unique hydrogen bonds formed between main chain of axial ligand Met59 and Gly50 on thermostability of Fe-Met coordination bond. This finding not only reveals the molecular mechanism responsible for thermostability of the coordination bond, but provides insight to design a heme protein that shows different function at different temperature.

P-055 Dynamic functional regulation of p38 MAP kinase

Yuji Tokunaga[1,2], Koh Takeuchi[3], Hideo Takahashi[3,4], and Ichio Shimada[1,3]
[1]Guraduate School of Pharmaceutical Sciences, The University of Tokyo
[2]Japan Biological Informatics Consortium (JBIC)
[3]Biomedicinal Information Research Center (BIRC), National Institute of Advanced Industrial Science and Technology (AIST)
[4]Graduate School of Nanobioscience, Yokohama City University

ABSTRACT

Mitogen-activated protein kinases (MAPKs) interact with various proteins, including upstream kinases, substrates, and phosphatases. Large part of these interactions is mediated through so-called "docking interactions", which utilize distal sites from the catalytic site of MAPKs. Although it has been disclosed that the docking interactions play a key role in defining the binding affinity and specificity, their effects on the structure and catalytic activity of MAPKs remain elusive. Here, we report an NMR analysis of active p38α MAPK dually phosphorylated on the conserved TXY motif. We found that the conformational transition of p38-2P to the "active conformation" requires both of the dual phosphorylation and adenosine phosphates-binding. Unexpectedly, the docking interaction with a p38-substrate, MK2, positively regulates the transition to the "active conformation" by increasing the affinity to adenine nucleotide by 7.5-fold. Correspondingly, k_{cat} for a substrate peptide phosphorylation catalyzed by p38-2P increased approximately 1.5-fold by the docking interaction. These findings underline the importance of the docking interactions in the regulation of the enzymatic function of p38 MAPK.

[1] ATP binding induces conformational change of p38-2P

To elucidate the structural basis of the activation mechanism of p38, dually phosphorylated p38 (p38-2P) was prepared by treating with its upstream kinase, MKK6. NMR spectral changes upon phosphorylation were restricted to the phosphorylation sites, indicating that p38-2P *per se* adopts an inactive conformation. To investigate if ATP binding induces a conformational rearrangement of p38-2P, NMR spectrum of p38-2P was recorded in the presence of ATP. It was essential to record 2D NMR spectra of p38-2P, under a dilute p38 concentration (~ 20 μM) and at low temperature (283 K) in about 30 minutes to avoid the ATP hydrolysis by p38-2P. To satisfy these restrictions, we employed methyl SOFAST-HMQC experiments. The amount of hydrolized ATP is less than 5% under this condition. A striking difference was observed between the spectra of p38-2P with and without ATP, as the majority of signals from methyl ^{1}H-^{13}C pairs of ILV residues exhibited chemical shift perturbations (Figure (a)). This reflects a global conformational change upon binding to ATP, supposedly corresponding to the domain closure and twisting motion between N- and C-lobes, as observed in the crystal structure of phosphorylated and AMP-PNP-bound p38γ. Therefore, a conformational transition of p38-2P to the "active conformation" is triggered by the cooperative action of the dual-phosphorylation and the binding of ATP. Furthermore, the "active

p38, active conformation, docking interaction

conformation" was also induced by ADP binding, indicating that the dissociation of the adenosine phosphates may trigger the active to inactive conformational transition.

[2] Docking interaction enhances adenosine phosphate-binding to p38-2P

To investigate the effect of the docking interaction on the conformational transition of p38-2P to it's "active conformation", ADP was titrated to p38-2P with or without a docking peptide derived from a native p38-substrate, MK2. ADP, instead of ATP, was used here as ADP-bound p38-2P also adopts the "active conformation" as discussed above without exhibiting hydrolysis. In both cases, dose-dependent spectral changes were observed for p38-2P in a slow exchange manner, however, the affinity was largely enhanced in the presence of the docking peptide. By analyzing the changes in the signal intensity, dissociation constants for ADP were determined to be 165 [μM] and 22 [μM] for the free and the peptide-bound states, respectively (Figure (b)). This indicates that the docking interaction with the substrate stabilizes the transition to the "active conformation". Such a regulation mechanism seems to be rational in that p38-2P preferably form an "active comformation" when bound to its native substrates.

[3] Docking interaction increases p38-2P kinase activity

To demonstrate the importance of docking interactions in the catalytic activity of p38-2P, we performed kinase assay of p38-2P. N-terminally GB1-tagged, 17-residue peptide derived from MK2 that contains a phosphoreceptor residue, Thr334, was used as a substrate. Without the docking peptide of MK2, p38-2P phosphorylated the substrate with a rate constant k_{cat} of 17.3 [/s] and a Michaelis constant K_m of 420 [μM]. When the MK2-derived docking peptide was supplemented, k_{cat} became 24.0 [/s], approximately 1.5-fold of enhancement (Figure (c)). This result agrees with the fact that p38-2P prefers the "active conformation" in the docking peptide-bound state, as shown above and underlines the function of the docking interaction in up-regulating catalytic activity of p38-2P.

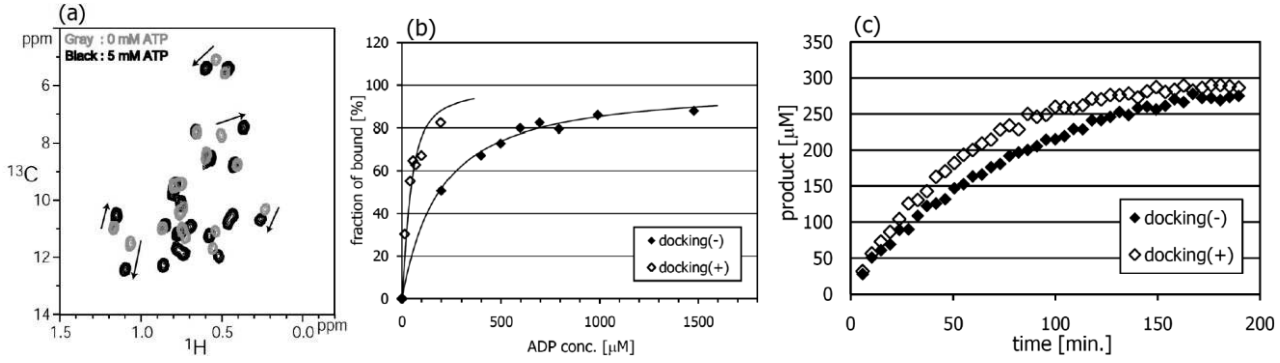

Figures. (a) ATP-induced spectral change of [ILV-methyl] p38-2P. Ile-δ1 region of ^{1}H-^{13}C HMQC spectra before and after addition of 5 mM ATP are shown in gray and black contours, respectively. Several chemical shift perturbations are indicated by arrows. (b) Result of ADP titrations. Bound fractions are plotted against ADP concentration. Bound fractions were determined based on the change in signal intensity derived from I84 located at the ATP-binding site. (c) Result of kinase assays. Concentrations of phophorylated product are plotted against reaction time. (b), (c) Symbols stand for the p38-2P states in the presence (open diamond) and absence (filled diamond) of MK2-derived docking peptide.

P-056 pKa measurement of acidic residues of equine β-lactoglobulin using 3D HCCO

Mitsuaki Nambo[1], Nobuaki Nemoto[2] and Masamichi Ikeguchi[1]
[1]Graduate School of Engineering, Soka University
[2]JEOL RESONANCE Inc.

β-lactoglobulin is a globular protein of 162 residues found in mammalian milk. Since equine β-lactoglobulin (ELG) was known to show several pH-dependent conformational transitions, we measured pKas of acidic residues to identify the residues related to these transitions. The pKas were determined from the pH titration experiments of side chain carboxyl carbon resonance using 3D HCCO, because ELG has many acidic residues (11 Asp and 16 Glu) and we couldn't resolve carboxyl carbon chemical shifts by 2D experiments.

Introduction

β-lactoglobulin is a major whey protein of 162 residues (18 kDa) belonging to the lipocalin family. ELG is an acidic protein including 11 aspartate (Asp) and 16 glutamate (Glu) residues (Figure 1). It has been known that ELG undergoes the acid denaturation and assumes non-native helical conformation (1). The pKa values of ionizable groups provide important information on the electrostatic environment of those residues, and are useful to understand the mechanism of acid denaturation of this protein. To know the pKa values of acidic residues, we have measured pH dependence of carboxyl carbon chemical shifts.

Material and Method

Fully $^{13}C/^{15}N$-labelled ELG was expressed in *E. coli*, and refolded in vitro. NMR spectra were acquired on a JEOL ECA-500 spectrometer equipped with z-gradient triple resonance probe. 3D-HCCO spectra were used for assignment of carboxyl carbon resonances and for monitoring their pH dependence.

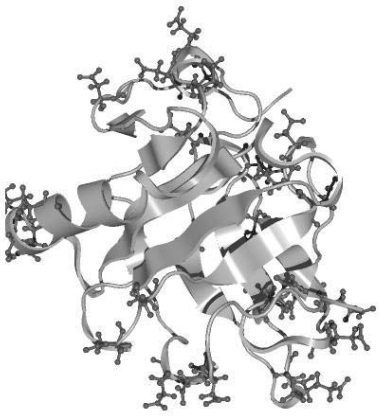

Fig.1. NMR structure of ELG. Acidic residues are indicated by ball-and-stick representation.

Results and discussion

We assigned chemical shift of side chain carboxyl carbon of all Asp residues (11/11) and 15 of 16 Glu residues based on previous assignments for chemical shifts of β or γ carbon and β or γ proton adjacent to carboxyl carbon. Unfortunately, signal of Glu89 was not detected probably due to broadening.

pH titration, pKa, beta-lactoglobulin, acidic residue, HCCO, stability

Thus, we monitored to chemical shifts of 26 residues from pH 2.6 to 9.1.

Residues especially perturbed are listed in Table 1, and their titration curves are shown in Fig. 2. The chemical shift of Asp98 does not change in the pH range observed, indicating that this residue is not titrated within this pH range. Because the chemical shift of Asp98 is within the range of values that other Asp residues show in the deprotonated state, the side chain of Asp98 seems to be still deprotonated at the lowest pH observed. Although Asp98 side chain conformation is not fixed in NMR structure (Figure 1), the corresponding residue of bovine β-lactoglobulin (BLG) forms hydrogen bonds with backbone amides of Lys101 and Tyr102 in crystal structures (2). These hydrogen bonds were not identified in NMR structures of BLG (3, 4). pKa is a useful information to check the side chain conformation determined by NMR.

The chemical shift of Asp90 also show little change in the pH range observed. Therefore, the pKa value of this residue is lower than 2.9. The structural explanation for this shifted pKa is also difficult from the NMR structure. In BLG, the corresponding residue is Asn. Because the denaturation midpoint of ELG is about pH 2.5 (1) and because BLG is stable at acidic pH, Asp90 may be responsible for the acid denaturation of ELG.

Table 1. pKa Values of acidic residue perturbed significantly[a]

Residue	pKa[b]	ΔpKa[c]
D33	4.65	0.85
E51	3.37	-1.13
D52	4.82	1.02
E55	2.95	-1.55
E68	3.51	-0.99
D90	<2.9	-
D96	3.02	-0.78
D98	<2.6	-

[a] A residue have absolute value of ΔpKa larger than standard deviation of all acidic residues.
[b] Uncertainty in pKa value is ±0.1.
[c] ΔpKa=pKa(native state)-pKa(model compound).

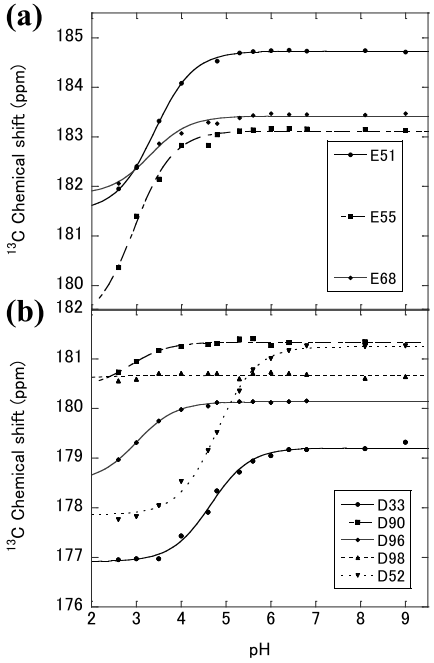

Fig.2. pH dependence of ^{13}C chemical shift of Glu C_δ(a) or Asp C_γ (b).

Reference

(1) Ikeguchi et al. (1997) Proteins 4; 567-575.
(2) Brownlow et al. (1997) Structure 5, 481-495
(3) Kuwata et al. (1999) Protein Sci. 8, 2541-2545
(4) Uhrínová et al. (2000) Biochemistry 39, 3565-3574

P-057 NMR analysis of interaction between an arginine-rich peptide and HIV-1 RRE RNA mutant

Tae Maeda[1], Maki Sugaya[2], Shoko Aoyama[2], Kazuo Harada[2] and Taiichi Sakamoto[1]
[1]Department of Life and Environmental Sciences, Faculty of Engineering, Chiba Institute of Technology and [2]Department of Life Sciences, Tokyo Gakugei University.

A short arginine-rich peptide derived from the HIV Rev protein is known to bind to an internal loop region of the Rev-responsive element (RRE) RNA. In the previous study, a high affinity RRE-binding peptide aptamer, referred to as K1 peptide, was shown to have low binding affinity towards the RRE_{AAC} mutant, in which G-G base pair in the internal loop is replaced by A-A base pair. Next, a high affinity peptide towards the RRE_{AAC} mutant has been selected from a random peptide library. The high affinity RRE_{AAC} aptamer, referred to as LDN1 peptide, was shown to have low affinity towards RRE. Thus, it was suggested that the K1 peptide and the LDN1 peptide recognizes G-G base pair and A-A base pair in the internal loop respectively.

In this study, NMR analysis was carried out to understand the structural basis of the recognition for A-A base pair by the peptide. Upon addition of the peptide to the RRE_{AAC}, the chemical shifts of lots of signals assigned to the internal loop region were changed. Furthermore, inter-molecular NOE was observed between the bulged A residue and the peptide. Compared to the previous study of the RRE-Rev peptide and RRE-K1 peptide interaction, LDN1 peptide seems to bind to large area of RRE_{AAC}.

INTRODUCTION

Interaction between arginine-rich peptides and their target RNAs have been useful model systems for the elucidation of general rules of RNA-protein interaction. The HIV Rev protein utilizes a short α-helical arginine-rich RNA-binding domain to bind to the major groove of an internal loop region of the Rev-response element (RRE) RNA (Fig. 1). A G-G base-pair which covaries to an isostructural A-A base pair has been shown to play an important structural role in Rev-RRE binding. In a previous study, a high affinity RRE-binding peptide aptamer, referred to as K1 peptide, was selected from combinatorial libraries using the bacterial two-plasmid system (1). Mutational

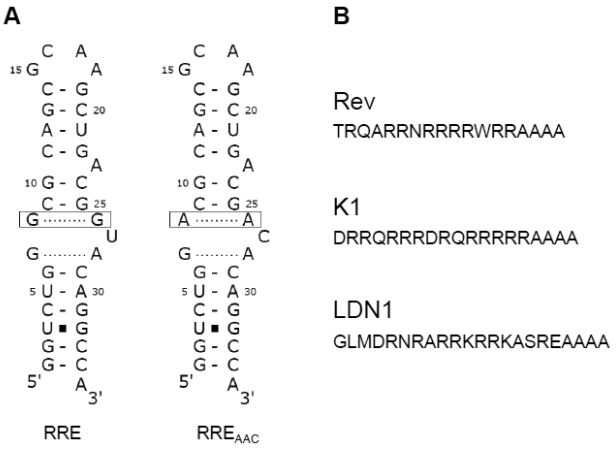

Fig. 1 The secondary structure of RRE and RRE_{AAC} mutant (A) and amino acid sequence of Rev, K1, and LDN1 (B).

Keyword: RNA, peptide, HIV

analysis of RRE showed that the K1 peptide has low binding affinity towards the RRE_{AAC} mutant, in which G-G base pair of the internal loop is replaced by A-A base pair (2). Thus, it was suggested that the K1 peptide recognizes G-G base pair in the internal loop of RRE. Furthermore, a high affinity RRE_{AAC} aptamer, referred to as LDN1 peptide, was selected and was shown to have low affinity towards RRE. The LDN1 peptide was found to bind to the internal loop region of the RRE_{AAC}, as in the case of the K1-RRE interaction. In this study, to investigate the structural basis of the recognition for G-G base pair by the K1 peptide and A-A base pair by the LDN1 peptide, NMR analysis of the interaction between the peptides and their target RNAs was carried out.

RESULTS AND DISCUSSION

The imino proton spectra of RRE and RRE_{AAC} were similar to each other, suggesting that the secondary structures of the both RNAs are similar to each other. To investigate the secondary structures of RRE and RRE_{AAC}, NOESY spectra were measured and imino proton signals were assigned. The imino proton signals of U3:G32 was identified by their unique chemical shifts and strong intra-base pair NOE. Starting from the unique signals, six signals were sequentially assigned by NOE connectivity as G1-G2-U3/G32-G31-U5. Furthermore, starting from a signal assigned to A-U base pair, three signals were sequentially assigned by NOE connectivity as U21-G13-G19. Although the imino proton resonances of G6, G7, G10, G15, G25, and G26 could not be observed or assigned because of broadening of the resonances or lack of NOE, NOE connectivities for imino proton resonances of G1-G2-U3/G32-G31-U5 and U21-G13-G19 revealed that two stems are formed as shown in Fig. 1A.

Upon addition of LDN1 peptide to RRE_{AAC}, imino proton signals of U5, G13, G19, U21 and G31 were perturbed and new signals were appeared (Fig. 2). Furthermore, in the NOESY spectrum of the complex, inter-molecular NOE was observed between the bulged A residue and the peptide. Compared to the previous study of the RRE-Rev peptide and RRE-K1 peptide interaction, LDN1 peptide seems to bind to large area of RRE_{AAC}.

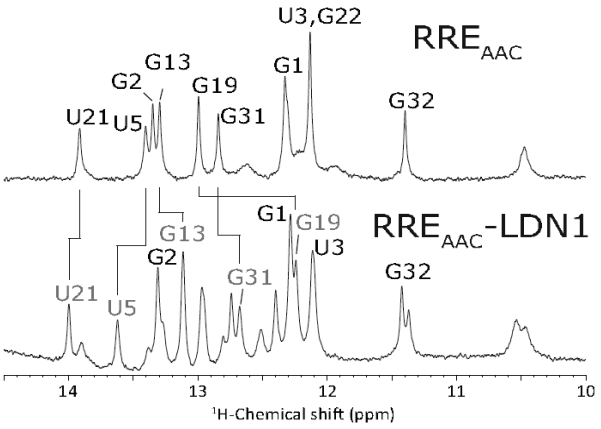

Fig. 2 1D imino proton spectra of RRE_{AAC} mutant

REFERENCES

1. Sugaya, M., Nishino, N., Katoh, A., Harada, K. *J. Pept.Sci.* **2008**, *14*, 924-935.
2. Sugaya, M., Nishimura, F., Katoh, A., Harada, K. *Nucleosides Nucleotides Nucleic Acids* **2008**, *27*, 534-545.
3. Aoyama, S., Sugaya, M., Kobayashi, C., Masuda, K., Maeda, T., Sakamoto, T., Kawai, G., Katoh, A., Harada, K. *Nucleic Acids Symp. Ser.* **2009**, 271-272.

P-058
Y

NMR Analysis on the Interaction between a Yeast Mitochondrial Oxidative Translocator Tim40/Mia40 and a FAD-Linked Sulfhydryl Oxidase Erv1

Takahiro Anzai[1], Shin Kawano[1], Ikuya Wakamori[1], Kayoko Terao[1] and Toshiya Endo[1]
[1]Department of Chemistry, Graduate School of Science, Nagoya University

An oxidative folding system has been recently discovered in the mitochondrial inter membrane space (IMS). Almost all the mitochondrial proteins including mitochondrial IMS proteins are synthesized in the cytosol and imported into mitochondria via the translocase of the outer membrane (TOM40) complex. Tim40/Mia40 introduces a disulfide bond into precursor IMS proteins as a substrate by forming a mixed disulfide-bond intermediate, which allows their oxidative folding. Erv1 is a FAD-linked sulfhydryl oxidase and specifically oxidizes reduced Tim40. We have succeeded in determination of the crystal structure of the "Tim40-substrate complex" as yeast Tim40 fusion proteins with a substrate peptide at N-terminus (MSP1-Tim40 and ITS-Tim40). Although high-resolution structures of Tim40 and Erv1 from other organisms are available, little is known about recognition and interactions between Tim40 and Erv1. Here we report the interaction analysis for Tim40 and Erv1 using PRE (paramagnetic resonance enhancement)-NMR.

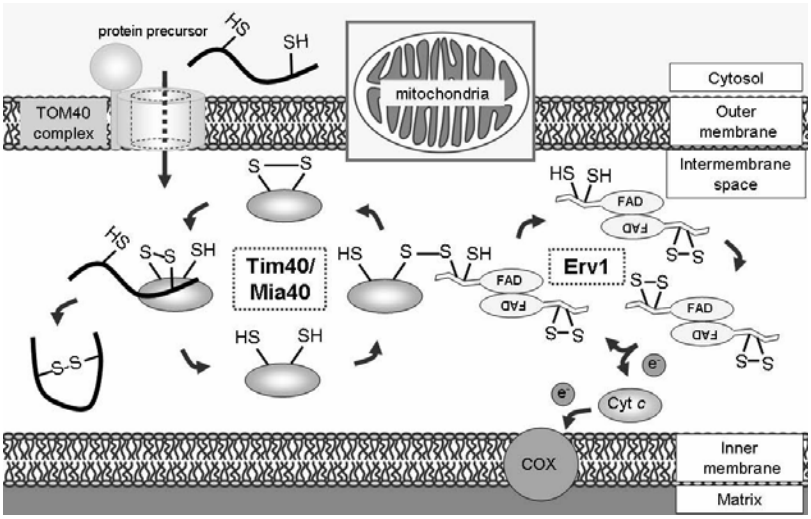

Fig.1, Tim40/Erv1 disulfide relay system

We prepared spin-labeled Erv1 (Erv1-MTSL((1-oxyl-2,2,5,5-tetramethyl- Δ 3-pyrroline-3-methyl) methanethiosulfonate)) and analyzed its interactions with Tim40, MSP1-Tim40 and ITS-Tim40. When we added increasing amounts of Erv1-MTSL to ^{15}N-labeled Tim40, its HSQC spectra with or without ascorbic acid were only slightly affected by Erv1-MTSL. In contrast, when we added Erv1-MTSL to ^{15}N MSP1-Tim40, we observed significant changes in its HSQC spectra with or without ascorbic acid In particular, signals from MSP1 and its nearby region of Tim40 were affected by Erv1-MTSL. Similarly, when we added Erv1-MTSL to ^{15}N ITS-Tim40, we observed significant changes in its HSQC spectra with or without ascorbic acid. These results suggest that Erv1 binds to the substrate and/or substrate-binding region of Tim40 and the substrate bound to Tim40 may enhance the interaction between Erv1 and Tim40.

mitochondria, disulfide-bond, PRE

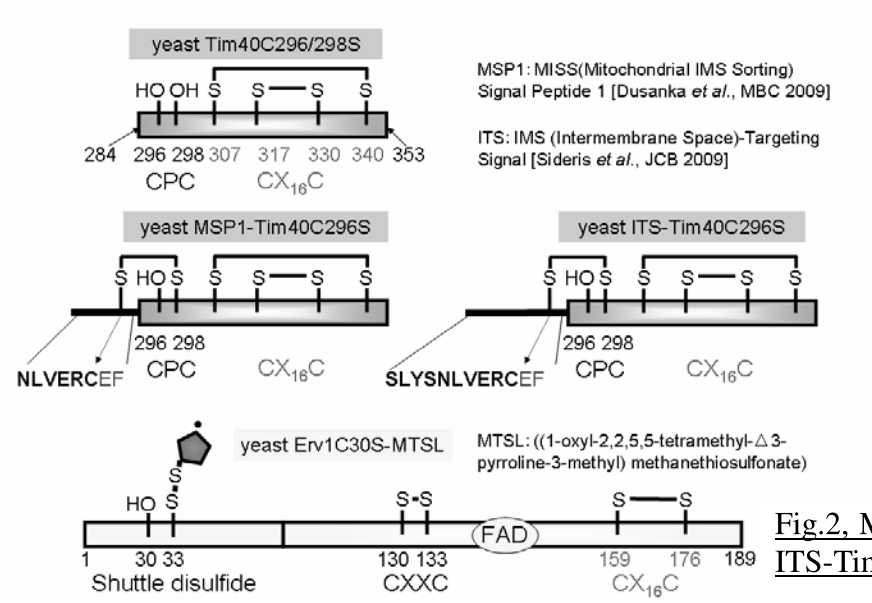

Fig.2, Models of Tim40, MSP1-Tim40, ITS-Tim40 and Erv1-MTSL

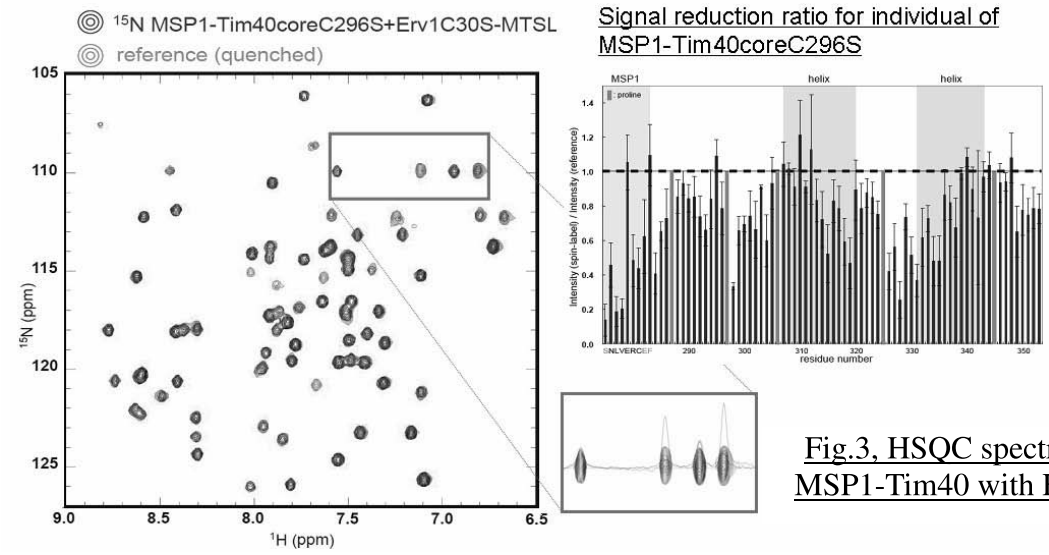

Fig.3, HSQC spectra of ^{15}N-labeled MSP1-Tim40 with Erv1C30S-MTSL

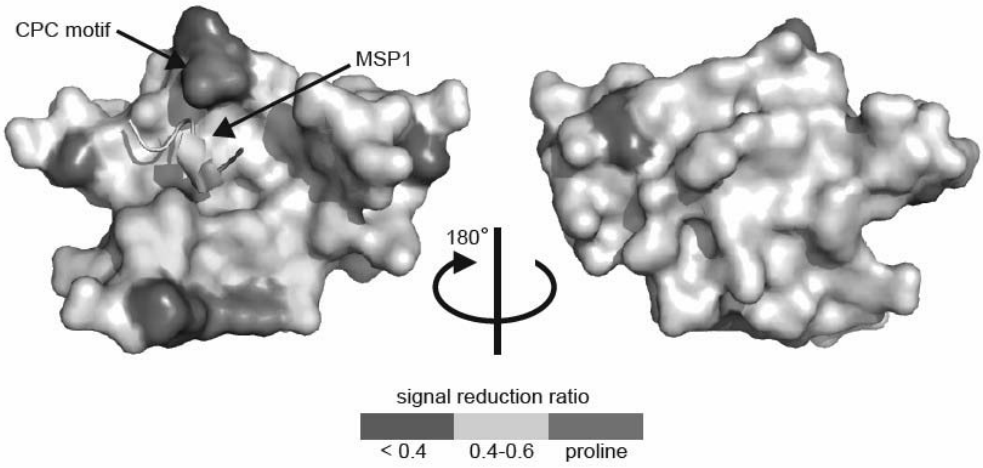

Fig.4, Mapping of signal reduction by spin-label on the crystal structure of MSP1-Tim40

P-059 Conformational fluctuation of Lys48-linked diubiquitin studied by high pressure NMR spectroscopy

Ryo Kitahara[1], Takashi Hirano[2] Maho Yagi-Utsumi[2,3], Kazumi Hata[1], Kazuyuki Akasaka[4] and Koichi Kato[2,3]

[1]College of Pharmaceutical Sciences, Ritsumeikan University, Japan
[2]Graduate School of Pharmaceutical Sciences, Nagoya-City University, Japan
[3]Okazaki Institute for Integrative Bioscience and Institute for Molecular Science, National Institutes of Natural Sciences
[4]High Pressure Protein Research Center, Kinki University, Japan

Here, we characterize conformational fluctuation of Lys48-linked linear diubiquitin, as a minimum model of polyubiquitin chains, by using high-pressure NMR spectroscopy. Comparing pressure induced changes in chemical shifts between mono-ubiquitin and diubiquitin at neutral pH, we found that pressure stabilizes the "open" orientation of the two subunits for diubiquitin. ^{15}N transverse relaxation constants R_2 indicate that both proximal and distal subunits exhibit the alternative conformation N_2 under high pressure, in which the helix swings slightly out with a simultaneous reorientation of the C-terminal segment, as observed in mono-ubiquitin under high pressure (Kitahara et al. J. Mol. Biol. 347, 277-285, 2005). We also conducted high pressure NMR experiments on Lys48-linked cyclic diubiquitin, in which Gly76 CO of each subunit and Lys48-sidechain of the other subunit is linked, as a model of the "closed" form of the Lys48-linked diubiquitin. Intriguingly, the N_1-to-N_2 conformational fluctuation could be retained in the individual subunit of cyclic diubiquitin. In addition, the interfacial hydrophobic groups between the subunits are hydrated and thus the cyclic diubiquitin takes a "semi-open" conformation under high pressure. These results suggest that the subunits of these diubiquitin share the same mode of conformational fluctuation with mono-ubiquitin, and the open-closed motion of diubiquitin could be coupled with the conformational fluctuation of subunits. We speculate that the intrinsic fluctuation of subunits or domains plays an essential role in the adaptation of global conformation of polyproteins and protein complex to the environment.

Introduction

Recently, experimental evidences for multiple conformations of proteins such as high Gibbs-free energy states of enzymes, partially unfolded states and MG states are increasing from a number of different sources including X-ray and NMR. The trend shows that multiple conformations are universal rather than exceptional for protein structure. However, despite significant progress in our understanding of conformational fluctuation of single domain proteins, the question concerning the characteristics of conformational fluctuation of polyproteins and protein complexes remains unanswered. Here, we study conformational fluctuation of Lys48-linked diubiquitin by using high pressure NMR spectroscopy combined with the molecular-selective isotope labeling technique. In particular, we investigate whether the N_1-N_2 conformational fluctuation is conserved in the two subunits of diubiquitin, as previously observed in mono-ubiquitin. Moreover, we investigate

Conformational fluctuation, high pressure, ubiquitin, diubiquitin, ^{15}N-R_2, chemical shifts

Fig.1 : K48-linked diubiquitin. (Left) open orientation. (Right) Closed orientation.

pressure dependence of "open"-"close" equilibrium of the Lys48-linked diubiquitin (Fig. 1).

In order to visualize the actual existence of conformational fluctuation, we apply pressure. Pressure shifts the water-protein system to a smaller volume within the range of its fluctuation, and, since the volume is strongly coupled to conformation, shifts the conformation within the range of its fluctuation. The higher is the pressure, the larger is the shift of the conformation. As many experiments show clearly, proteins in solution, in principle, unfold under high pressure. Thus we can postulate that the partial molar volume of a protein molecule decreases in parallel with the loss of the conformational order (the volume theorem). The volume decrease along unfolding is due probably to the loss of cavities in the protein interior and hydration. We may extend the theorem into the protein complex and polymer forms.

Results and Discussion

We prepared Lys48-linked diubiquitin, in which the proximal or distal subunit is selectively ^{15}N labelled. We also created Lys48-linked cyclic diubiquitin, in which Gly76 CO of each subunit and Lys48-sidechain of the other subunit is linked. The cyclic diubiquitin is thought to mimic the "closed" orientation of the Lys48-linked diubiquitin, while the mono-ubiquitin is a model of the "open" orientation. We performed $^{15}N/^{1}H$ HSQC measurements for these diubiquitin at different pressure from 30 to 3000 bar on a DRX-500 and DRX-600 spectrometer. Comparing ^{1}H and ^{15}N chemical shifts between mono-ubiquitin and distal/proximal subunit of diubiquitin, large chemical shifts are observed at many residues, indicating a presence of the "open"-"close" equilibrium of the Lys48-linked diubiquitin. Although the predicted interface of the two subunits is consistent with that predicted by X-ray crystallography, the "open" orientation of diubiquitin is substantially populated in solution (Hirano et al. *in press*). Pressure dependence of the chemical shifts indicates that the open orientation could be dominantly populated in diubiquitin under high pressure. Large R_2 values are observed at several residues in α-helix and β-sheet region of the proximal and distal subunits, as observed in mono-ubiquitin under high pressure. This result indicates that alternative conformation N_2 is stabilized in both proximal and distal subunits under high pressure, in which the α-helix swings slightly out with a simultaneous reorientation of the C-terminal segment. Similar results are observed in the cyclic diubiquitin, indicating that the interfacial hydrophobic groups between the subunits are hydrated and thus the cyclic diubiquitin takes a "semi-open" conformation under high pressure. Since the "open"-"close" transition of diubiquitin and N_1-N_2 conformational transition within the subunits are observed at similar pressure region, the open-closed motion of diubiquitin could be coupled with the conformational fluctuation of subunits. We speculate that the intrinsic fluctuation of subunits or domains plays an essential role in the adaptation of global conformation of polyproteins and protein complex to the environment.

P-060

An extensively hydrated and folded conformer stabilized at high pressure and low temperature. The case of c-Myb R2 sub-domain.

Sunilkumar P. N.[1,2], Akihiro Maeno[1,2], Hiroshi Matsuo[2], Masayuki Oda[3], Hisayuki Morii[4] and Kazuyuki Akasaka[2]

[1]Graduate School of Biology-Oriented Science and Technology, Kinki University, 930 Nishimitani, Japan.

[2]High Pressure Protein Research Center, Institute of Advanced Technology, Kinki University, 930 Nishimitani, Japan.

[3]Graduate School of Life and Environmental Sciences, Kyoto Prefectural University, Kyoto, Japan.

[4]National Institute of Advanced Industrial Science and Technology (AIST), Tsukuba, Japan.

Proteins usually exist in solution as equilibrium of different conformers including the major basic folded conformer, minor populations of other folded conformers which may be very crucial for function and fully unfolded conformer (1-6). The low populated hidden conformers are seldom detected and characterized by normal spectroscopic methods. Variable pressure techniques are very useful for the study of protein conformational equilibrium within the folded state ensemble (5-10). c-Myb is a transcription factor involved in proliferation and differentiation of hematopoietic cells (11-14). The DNA-binding domain of c-Myb consists of three structural repeats, R1, R2 and R3, of 51-52 amino acids, each forming a helix-turn-helix related motif containing three helices (15, 16). Three conservative tryptophans in each repeat participate in forming a hydrophobic core, which definitely characterizes the structure of the repeat. Comparison of the three repeat structures indicates that there exists a large cavity in the hydrophobic core of R2 (90-141 segment) and upon DNA binding the Trp95 side-chain is sliding into its internal cavity, which requires high conformational flexibility of R2 (17). The side-chain of Val103 is directly orienting to the internal cavity. V103L mutation fills the cavity and reduces the conformational flexibility of R2 and also the DNA binding activity of c-Myb protein (17, 18). The primary aim of this study is to search for low populated conformer(s), in addition to the basic folded structure, of c-Myb R2 sub-domain which may be more amenable to DNA binding. The second objective is to check the efficacy of the combination of variable pressure fluorescence and NMR techniques to find out such conformers.

Keywords: High pressure NMR, Hydration, High energy conformer

We have used a chemically stable pseudo wild-type of c-Myb R2 sub-domain with C130I mutation (WT*), retaining the large internal cavity and its cavity-filled V103L mutant. These two proteins have been obtained by solid phase peptide synthesis using F-moc chemistry strategy. Variable-pressure Trp fluorescence (3 to 600 MPa) and ^{1}H-NMR (3 to 300 MPa) have been carried out on the WT* and V103L proteins at pH 7.5 and temperature 5°C.

Change in the combined fluorescence emission maximum (λ_{max}) of all the three Trp residues in WT*, with pressure (from 3 to 600 MPa), is shown in **Figure 1b**. The λ_{max} value shows a significant red shift from 342 nm to ~355 nm as pressure is increased from 3 to 300 MPa and it remains constant up to 600 MPa. All the three Trp side-chains occupying the core of the R2 structure (cf. **Fig. 1a**; PDB ID: 1GV5) are in fully hydrated state at 300 MPa, as indicated by a λ_{max} of ~355 nm. This often happens when the protein is in a fully unfolded state and the Trp side chains are fully exposed to water. An array of 1D - ^{1}H NMR spectra of the WT*, at different pressures ranging from 3 to 300 MPa, is shown in **Fig.1c**. It shows continuous shifts of the high-field shifted methyl signals, characteristic of the hydrophobic core, toward still higher field without much intensity change indicating that the protein remains folded with a compaction of the core at 300 MPa. This discrepancy between Trp fluorescence and NMR results can happen only if water penetrates into the core of the folded protein and hydrates the Trp side-chains. Thus, the Trp fluorescence and ^{1}H NMR results together suggest the existence of a peculiar conformer (N') at 300 MPa that is extensively hydrated, but, on average, folded in addition to the basic folded conformer (N).

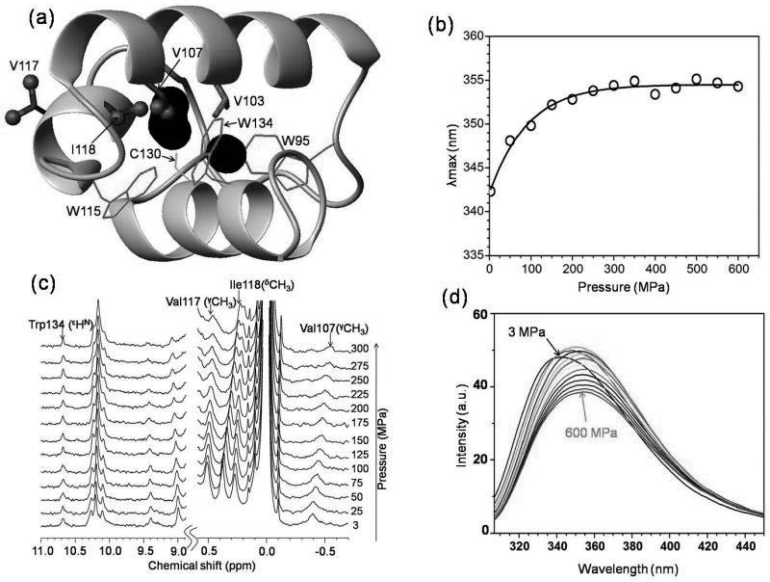

Figure 1: (a) Three- dimensional structure of c-Myb R2 sub-domain (PDB ID: 1GV5). Cavity positions are colored black. The mutation site V103 is colored magenta. The three Trp side chains are colored red. The side chain methyl groups which have been assigned in the NMR spectrum are shown as brown balls. C130 residue side chain is colored yellow. (b) Change in Trp fluorescence emission maximum (λ_{max}) of WT* protein as a function of pressure. (c) 1D-^{1}H NMR spectra of WT* protein at various pressures from 3 to 300 MPa. (d) Trp fluorescence emission spectra of WT* protein at various pressures from 3 to 600 MPa.

Presence of the second conformer (N') has been further supported by the non-linear nature of the pressure induced chemical shift changes (8, 19). The pressure induced changes in the well isolated signals of the side chain groups, Val107 ($^{\gamma}CH_3$), Ile118 ($^{\delta}CH_3$) and Trp134 ($^{\varepsilon}H^N$), occupying the core of the protein and that of Val117 ($^{\gamma}CH_3$) occupying the periphery of the protein (cf. **Fig. 1a**), but close to Tyr110 ring, are marked in **Fig.1c**. The pressure induced chemical shift changes of the side chain signals occupying the structural core are clearly non-linear with sigmoidal character, centering around 150 MPa, and are found at different parts of the protein molecule. This indicates that the WT* protein is co-operatively undergoing conformational transition to a second state along with the general core compaction. The pressure induced changes in chemical shifts of the V107 ($^{\gamma}CH_3$) and I118 ($^{\delta}CH_3$) groups, which are very close to the internal cavity and also to the side chain indole rings of W115 and W134, are shown in **Figure 2a & b.** These results indicate that the native folded conformer N of R2 is in equilibrium with another folded conformer N'. And also, many of the NMR signals show considerable line broadening with pressure indicating that N' is heterogeneous and has higher conformational flexibility than N (cf. **Fig 1c**).

In the case of the cavity filled V103L mutant the Trp fluorescence λ_{max} is shifted from 341 to ~346 nm at 300 MPa, which remains almost the same up to 600 MPa. The non-linear nature, with sigmoidal character, of the pressure induced chemical shift changes of Val107 ($^{\gamma}CH_3$) and Ile118 ($^{\delta}CH_3$) ^{1}H NMR signals indicates that a conformational change is taking place in addition to the general compaction of the protein molecule. These results indicate that the pressure stabilized conformer of the cavity filled R2 is not extensively hydrated. We conclude that the highly flexible extensively hydrated folded state N' of the R2 sub-domain is intimately related to the hydration of its large internal cavity.

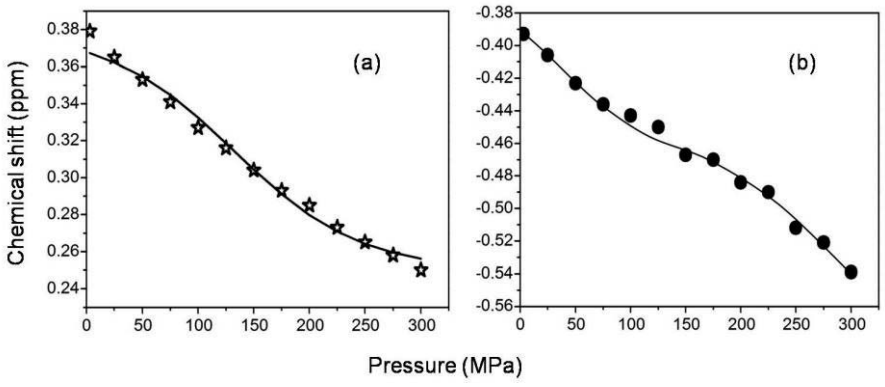

Figure 2: (a) Change in chemical shift of Ile118 ($^{\delta}CH_3$) group peak in WT* protein as a function of pressure from 3 to 300 MPa. (b) Change in chemical shift of Val107 ($^{\gamma}CH_3$) group peak in WT* protein as a function of pressure from 3 to 300 MPa.

The sliding process of the Trp95 side-chain into the internal cavity present in the R2 sub-domain (17) requires high conformational flexibility of R2. The increased conformational flexibility of the extensively hydrated folded N' state prompted us to speculate that this newly identified state of R2 is likely to be involved in the DNA binding process rather than the basic folded native conformer N. This novel extensively hydrated folded state of a globular protein, predicted from pressure perturbation studies, is considered rather universally present in globular proteins having internal cavities. The presence of cavity hydrated low lying excited states in hen lysozyme has been identified at high pressure and low temperature (7), which supports the previous statement. And also we propose that a combination of fluorescence and NMR, at high pressure and low temperature, is an efficient method for the identification of low populated extensively hydrated folded states in globular proteins.

References:

1. Bernadó P. and M. Blackledge (2010). *Nature*. 468:1046–1048.
2. Woodward, C., I. Simos, and E. TuÈchsen (1982). *Mol. Cell. Biochem.* 48:135-160.
3. Li, R., and C. Woodward (1999). *Protein Sci.* 8:1571-1591.
4. Rumbley, J., L. Hoang, …, S. W. Englander (2000). *Proc. Natl. Acad. Sci. U.S.A.* 98:105-112.
5. Kitahara, R., S. Sareth, …, K. Akasaka (2000). *Biochemistry*, 39:12789-12795.
6. Kitahara, R., H. Yamada, and K. Akasaka (2001). *Biochemistry*, 40: 13556-13563.
7. Kamatari, Y. O., L. J. Smith, …, K. Akasaka (2011). *Biophys. Chem*. 156: 24–30.
8. Akasaka, K. and H. Li (2001). *Biochemistry*.40:8665-8671.
9. Akasaka, K (2006). *Chem. Rev.* 106: 1814−1835.
10. Panick, G., G. J. A. Vidugiris, …, C. A. Royer (1999). *Biochemistry*. 38: 4157-4164.
11. Ness S. A. (1999). *Oncogene.*18:3039-3046.
12. Introna, M., and J. Golay (1999). *Leukemia*.13:1301- 1306.
13. Ganter, B., and J. S. Lipsick (1999). *Adv. Cancer. Res.* 76:21-60.
14. Tomita, A., T. Wantanabe, …, H. Saito (1998). *Leukemia*.12:1422-1429.
15. Gonda, T. J., N. M. Gough, …, J. de Blaquiere (1985). *EMBO J.* 4: 2003-2008.
16. Klempnauer, K.-H., and A. E. Sippel (1987). *EMBO J.* 6: 2719-2725.
17. Ogata, K., C. Kanei-Ishii, …, Akinori Sarai (1996). *Nature Struct. Biol*. 3:178 - 187.
18. Morii, H., H. Uedaira, …, A. Sarai (1999). *J. Mol. Biol.* 292: 909-920.
19. Akasaka, K., H. Li, …, C. K. Woodward (1999). *Protein Sci*. 8: 1946-1953.